

No Minima, No Collisions: Combining Modulation and Control Barrier Function Strategies for Feasible Dynamical Collision Avoidance

Yifan Xue[†] and Nadia Figueroa[†] *Member, IEEE*

Abstract—As prominent real-time safety-critical reactive control techniques, Control Barrier Function Quadratic Programs (CBF-QPs) work for control affine systems in general but result in local minima in the generated trajectories and consequently cannot ensure convergence to the goals. Contrarily, Modulation of Dynamical Systems (Mod-DSs), including normal, reference, and on-manifold Mod-DS, achieve obstacle avoidance with few and even no local minima but have trouble optimally minimizing the difference between the constrained and the unconstrained controller outputs, and its applications are limited to fully-actuated systems. We dive into the theoretical foundations of CBF-QP and Mod-DS, proving that despite their distinct origins, normal Mod-DS is a special case of CBF-QP, and reference Mod-DS’s solutions are mathematically connected to that of the CBF-QP through one equation. Building on top of the unveiled theoretical connections between CBF-QP and Mod-DS, reference Mod-based CBF-QP and on-manifold Mod-based CBF-QP controllers are proposed to combine the strength of CBF-QP and Mod-DS approaches and realize local-minimum-free reactive obstacle avoidance for control affine systems in general. We validate our methods in both simulated hospital environments and real-world experiments using Ridgeback for fully-actuated systems and Fetch robots for underactuated systems. Mod-based CBF-QPs outperform CBF-QPs as well as the optimally constrained-enforcing Mod-DS approaches we proposed in all experiments.

I. INTRODUCTION

Recent developments in autonomous systems have brought increasing research efforts into the field of robot obstacle avoidance and safe control system design. Autonomous robots colliding with environmental obstacles or their co-workers would not only reduce work efficiency but also injure users in safety-critical tasks ranging from autonomous driving to household human-robot cooperation [1]. In literature, collision-free guarantees in dynamic environments are achieved either through the satisfaction of constraints in optimization-based approaches [2, 3, 4, 5, 6, 7] or through reactive potential-field inspired closed-form solutions [8, 9, 10, 11, 12, 13, 14, 15]. Quadratic Programming based Control Barrier Functions (CBF-QP) [2] and Dynamical System motion policy modulation (Mod-DS) [11] are two notable methods for modifying an agent’s nominal controller from these categories, respectively.

CBF-QP minimally adjusts a nominal controller while ensuring safety through affine inequality constraints in the context of set invariance [2]. Mod-DS, inspired by Harmonic Potential

functions [10] [13], is one of the state-of-the-art closed-form approaches in obstacle avoidance, which eliminated the excessive local minima faced by Artificial Potential Fields (APF) [8] and can be generalized to different environments more easily than navigation functions [9]. Mod-DS, initially introduced in [11] for convex obstacle avoidance reshapes a desired motion vector field to circumnavigate obstacle boundaries using the geometry of the collision surface through a *modulation* matrix, which we referred as “normal Mod-DS” in the paper. It was later extended by [13] to “reference Mod-DS”, which handles star-shaped obstacles with impenetrability and (almost) global convergence guarantees, and by [16] to “on-manifold Mod-DS”, which realizes local-minimum-free obstacle avoidance for all obstacle geometries in fully actuated systems. While Mod-DS approaches are highly reactive, limited by their closed-form nature, they cannot straightforwardly account for input or kinematic/dynamic constraints like CBF-QP, and are more likely to cause collisions in scenarios where the robot is tightly squeezed between multiple obstacles. Moreover, the application of Mod-DS approaches is so far limited to fully actuated systems. CBF-QP, contrarily, holds the advantage of working for control affine systems in general but suffers from local minimum issues facing all obstacle geometries, even convex ones.

With the emergence of different safety-critical control approaches, several attempts have been made to compare them. For example, [17] compared CBF-QP with APF in static environments with convex obstacles and analytically proved that APF is a special case of CBF-QP. [18] compares the performance of CLF-CBF QP with Hamilton-Jacobi reachability analysis in environments with static unsafe sets. Others draw comparisons between optimization-based safe control approaches with deep neural networks, such as [19], which studies the differences between deep learning and MPC for adaptive cruise control. Despite these efforts, a comprehensive analysis on general obstacle avoidance techniques in real-time dynamic settings is missing. Although Mod-DS has risen in popularity in recent years due to its simplicity of computation and strong theoretical guarantees proving that collision-free trajectories can be replanned in real-time without introducing topologically (unnecessary) minima or increased execution time [13, 14, 16], it is rarely included in such comparisons. Furthermore, when choosing between reactive safe controllers like Mod-DS and CBF-QP, users are forced to make tradeoffs between the ability to enforce complicated input and multi-obstacle constraints and the reduction of local minima, no

[†]Y. Xue and N. Figueroa are with the Department of Mechanical Engineering and Applied Mechanics, University of Pennsylvania, Philadelphia, PA 19104 USA {yifanxue, nadiafig}@seas.upenn.edu

existing safe reactive controller is able to combine the strength of both CBF-QP and Mod-DS approaches to achieve local-minimum free and constraints-flexible obstacle avoidance for control affine system in general.

In this work, our analysis focuses on comparing Mod-DS and CBF-QP because they generate feasible obstacle-avoiding motion policies within 10 ms, as required by the dynamic environment of interactive robot tasks. Analyzing and understanding the behavioral similarities, differences, and theoretical connections between CBF-QP and Mod-DS approaches then sets the base for our proposal of Mod-based CBF-QP controllers, which embody the strength of both. The storyline of the paper is organized as follows: first, we quantitatively and qualitatively compare CBF-QP and Mod-DS variants with one another to unveil the behavior differences and similarities shared by them. For example, all CBF-QP and Mod-DS approaches, except for on-manifold Mod-DS, are subject to local minima caused by collinearity issues. Through the analysis, we conclude that Mod-DS provides a much higher target-reaching rate than CBF-QP, and is the preferred approach for safe navigation in concave-obstacle environments using fully actuated systems. Some might argue that Mod-DS approaches, suffering from closed-form safe control methods' common weakness in handling input constraints, are less practical than CBF-QP in real-life navigation tasks. Therefore, we propose speed-constraining and velocity-constraining strategies that enable Mod-DS to trivially enforce input constraints in fully-actuated systems, as the second contribution of the work. Then building on top of the observations, we prove theoretically that normal Mod-DS and CBF-QP are equivalent in single obstacle avoidance settings for fully actuated systems, and that reference Mod-DS solutions can be mathematically connected to CBF-QP using a one-line equation. Finally, based on the theoretical connections deduced, we propose reference and on-manifold Mod-based CBF-QP controllers as the most important contribution of our paper. The proposed Mod-based QP methods not only inherit CBF-QP's strength in handling complicated constraints, but are also able to reduce local minima to be no more than their corresponding reference and on-manifold Mod-DS approaches. Moreover, on-manifold Mod-based CBF-QP methods, like CBF-QP, are applicable to control affine systems in general. All methods proposed, including constraint-enforcing Mod-DS and Mod-based CBF-QP, are validated in multiple challenging concave and dynamic obstacle environments using the Ridgeback and Fetch robots, in which Mod-based CBF-QP controllers easily outperform both CBF-QP and Mod-DS approaches.

Contributions: Following we summarize our major contributions:

- 1) A theoretical and practical analysis, equivalence and comparison of Mod-DS vs. CBF-QP (section IV, section V).
- 2) A novel constraint-enabled Mod-DS approach tailored for omni-directional robots, incorporating speed and velocity limits in its closed-form solution. We show that this approach matches the performance of velocity-constrained CBF-QP and is computationally efficient (section VI).
- 3) Novel Mod-based CBF-QP controllers that achieves respectively local-minimum-reduction and local-minimum-

free obstacle avoidance for control affine system in general (section VII).

- 4) Extensive validation of the proposed constraint-enabled Mod-DS and Mod-based CBF-QP on simulations and real hardware experiments (section VIII).

II. PROBLEM STATEMENT

A. Safety-Critical Control for Dynamic Obstacle Avoidance

Both subjects of the work, Mod-DS and CBF-QP, define the notion of robot safety and generate safe control algorithms based on boundary functions. Given a continuously differential function h , state $x \in \mathbb{R}^d$ and time $t \in \mathbb{R}$, $h : \mathbb{R}^d \rightarrow \mathbb{R}$ is a boundary function if the safe set C (outside the obstacle), the boundary set ∂C (on the boundary of the obstacle), and the unsafe set $\neg C$ (inside the obstacles) of the system can be defined as in (1), (2), (3) [2]. The boundary function h is time-dependent for scenarios where the unsafe set are moving. In static obstacle avoidance, boundary function $h(x, t) = h(x)$.

$$C = \{x \in \mathbb{R}^d : h(x, t) > 0\} \quad (1)$$

$$\partial C = \{x \in \mathbb{R}^d : h(x, t) = 0\} \quad (2)$$

$$\neg C = \{x \in \mathbb{R}^d : h(x, t) < 0\} \quad (3)$$

In practice, $h(x, t)$ is often measured as the distance from the controlled agent to the obstacle surface boundary, i.e. the signed distance function. Given environments defined by boundary functions, the goal of a safety-critical controller is to generate an admissible input u that will ensure the state of the robot x is always within the safe set C and eventually reaches a target state $x^* \subset C \in \mathbb{R}^d$.

B. Notations

In this work, we use notation $\|\cdot\|_p$ to represent the p-norm of a vector and denote $\|\cdot\|_p^q = (\|\cdot\|_p)^q$, $\forall p, q \in \mathbb{R}^+$. We annotate $\langle a, b \rangle$ for the dot product between vectors a and b . $\mathbf{0}_{a \times b}$ is a matrix full of 0s of size $a \times b$. Given a vector $a(\cdot)$, \hat{a} represents the axis whose direction is the same as $a(\cdot)$, and $a[:k]$ represents the new vector formed by the first k elements in a .

C. Assumptions

Safe Controller: The safe-controller u takes as input the current state x , the nominal control u_{nom} , and outputs the desired safe control input to the system, based on the robot's knowledge of the environment given by the obstacle boundary function $h(x, t)$. In Section IV and VI, u_{nom} is defined assuming single integrator agent dynamics, while in Section VIII we formulate u_{nom} to approximate linear dynamical systems assuming higher order control systems; i.e., Dubin's car.

Obstacle Shapes: In this work, we analyze and propose safe control methods facing all obstacle geometries, including convex, star-shaped, and non-star-shaped concave obstacles. Star-shaped obstacles are defined as concave obstacles that have a reference point inside the obstacle, from which all rays cross the boundary only once [20]. Without loss of generality to applications in higher-dimensional state space,

the method compared and proposed are showcased in 2D navigation and manipulation tasks. We define $x_{\text{rel}} \in \mathbb{R}^2$ as the robot position measured in the obstacle based frame, varying based on the geometric center, and orientation of the obstacle. Safe controllers' abilities in navigating around convex obstacles are tested using a circle with boundary function h_{conv} defined as in (4), where $c_r \in \mathbb{R}^+$ is the radius of the circle.

$$h_{\text{conv}}(x_{\text{rel}}) = \|x_{\text{rel}}\|_2 - c_r \quad (4)$$

Likewise, star-shaped obstacles are defined using a funnel-shape with boundary function h_{star} as in (5), where $C_a \in \mathbb{R}^2$ and $c_b \in \mathbb{R}^+$ are constants.

$$h_{\text{star}}(x_{\text{rel}}) = \|x_{\text{rel}} - C_a\|_4 - c_b \quad (5)$$

Finally, non-star-shaped obstacles are represented using boundary function h_{nstar} learned using Gaussian Process Distance Field (GPDF) of a C-shape. Isoline maps showing the change in h values with respect to the relative location of the agent can be found in Fig. 1. $h(x, t)$ functions for convex, star and non-star shapes are constructed to align with the safe set definition in Eq. (1), (2), and (3). Here we limit the scope of our discussion to cases where the size of the obstacles is fixed with no shrinkage, expansion, or deformation. All moving (i.e. time t dependent) obstacles exhibit only translation and rotational motion.

III. PRELIMINARIES

A. Boundary Function Requirement

According to [2] and [11, 13, 14], CBF-QP and Mod-DS method share the same requirement for the boundary function $h(x, t)$: $h(x, t)$ must be a continuously differentiable function of class \mathcal{C}^1 satisfying safe set definitions in Eq. (1), (2) and (3).

B. Control Barrier Functions

In CBF-QP formulation, the boundary function $h(x, t)$ is also called the barrier function. To guarantee safety of the controlled agent, CBF-QP utilizes the Nagumo Set Invariance Theorem.

Definition 3.1 (Nagumo Set Invariance)

$$C \text{ is set invariant} \iff \dot{h}(x, t) \geq 0 \quad \forall x \in \partial C \quad (6)$$

Control Barrier Functions are designed by extending Nagumo set invariance theorem to a "control" version[2], where the condition $\forall x \in \partial C$ is rewritten mathematically using an extended \mathcal{K}_∞ function α ,

$$C \text{ is set invariant} \iff \exists u \text{ s.t. } \dot{h}(x, u, t) \geq -\alpha(h(x, t)). \quad (7)$$

Definition 3.2 (Extended \mathcal{K}_∞ Functions) An extended \mathcal{K}_∞ function is a function $\alpha : \mathbb{R} \rightarrow \mathbb{R}$ that is strictly increasing and with $\alpha(0) = 0$; that is, extended \mathcal{K}_∞ functions are defined on the entire real line $(-\infty, \infty)$.

Control barrier functions can be generalized to any nonlinear affine systems of the form in (8), where $x \in \mathbb{R}^d, u \in \mathbb{R}^p$, and

f, g are Lipschitz continuous. The CBF conditions in (7) can be used to formulate a quadratic programming problem that guarantees safety by enforcing the set invariance of the safety set C defined in (1). For general control affine systems, CBF-QP is defined as in (9).

$$\dot{x} = f(x) + g(x)u \quad (8)$$

$$u_{\text{cbf}} = \arg \min_{u \in \mathbb{R}^p} \frac{1}{2} \|u - u_{\text{nom}}\|_2^2$$

$$L_f h(x, t) + L_g h(x, t)u + \frac{\partial h(x, t)}{\partial t} \geq -\alpha(h(x, t)) \quad (9)$$

For fully-actuated systems in (10), where $x, u \in \mathbb{R}^d$, the special case of CBF-QP can be simplified as in (11).

$$\dot{x} = u \quad (10)$$

$$u_{\text{cbf}} = \arg \min_{u \in \mathbb{R}^d} \frac{1}{2} \|u - u_{\text{nom}}\|_2^2$$

$$\nabla_x h(x, t)^\top u + \frac{\partial h(x, t)}{\partial t} \geq -\alpha(h(x, t)) \quad (11)$$

Closed-Form Solution: CBF-QP has closed-form solutions in single obstacle environments when robot input limitations are ignored. Solving the convex optimization problem in (9) and (11) using KKT conditions, the explicit CBF-QP solutions are respectively (12) and (11). For simplicity of the solutions, we abuse notations and let $\alpha = \alpha(h(x, t)) + \frac{\partial h(x, t)}{\partial t}$, $L_f h = L_f h(x, t)$, $L_g h = L_g h(x, t)$ and $\nabla_x h = \nabla_x h(x, t)$.

$$u_{\text{cbf}} = \begin{cases} u_{\text{nom}} & \text{if } L_f h + L_g h u_{\text{nom}} \geq -\alpha \\ u_{\text{nom}} - \frac{L_f h + L_g h u_{\text{nom}} + \alpha}{L_g h} L_g h^\top & \text{otherwise} \end{cases} \quad (12)$$

$$u_{\text{cbf}} = \begin{cases} u_{\text{nom}} & \text{if } \nabla_x h^\top u_{\text{nom}} \geq \alpha \\ u_{\text{nom}} - \frac{\nabla_x h^\top u_{\text{nom}} + \alpha}{\nabla_x h^\top \nabla_x h} \nabla_x h & \text{otherwise} \end{cases} \quad (13)$$

C. Mod-DS Approach

Unlike CBF-QP that works for control affine systems in general, Mod-DS can only be adopted in fully actuated systems described in (10).

In Mod-DS, obstacle avoidance is achieved by multiplying a full-rank locally active matrix $M(x, t) \in \mathbb{R}^{d \times d}$ to a nominal DS \dot{x}_{nom} and reshaping the flow by reducing the relative speed of the robot towards the obstacle, while increasing or maintaining the speed in the directions tangent to the obstacle surface represented by $h(x, t)$. Mod-DS is computed for moving obstacles as [13, 14],

$$u_{\text{mod}} = \dot{x}_{\text{mod}} = M(x, t)(\dot{x}_{\text{nom}} - \dot{x}_o) + \dot{x}_o \quad (14)$$

$$\dot{x}_o = \dot{x}_L^o + \dot{x}_R^o \times (x - x_o), \quad (15)$$

where x_o is an obstacle's axis of rotation where its motion can be characterized about, $\dot{x}_L^o, \dot{x}_R^o \in \mathbb{R}^d$ are the linear and angular velocity vector of the obstacle with respect to point x_o . In a static scenario, Eq. (16) reduces to $\dot{x} = M(x)\dot{x}_{\text{nom}}$.

$M(x, t)$ is constructed analogous to an Eigendecomposition, where $E(x, t) \in \mathbb{R}^{d \times d}$ is the basis matrix and $D(x, t) \in \mathbb{R}^{d \times d}$ is the diagonal scaling matrix. The basis matrix $E(x, t)$ consists of a direction vector facing the obstacle $d(x, t) \in \mathbb{R}^{d \times 1}$ and a hyperplane $H(x, t) \in \mathbb{R}^{d \times (d-1)}$ tangent to $h(x, t)$.

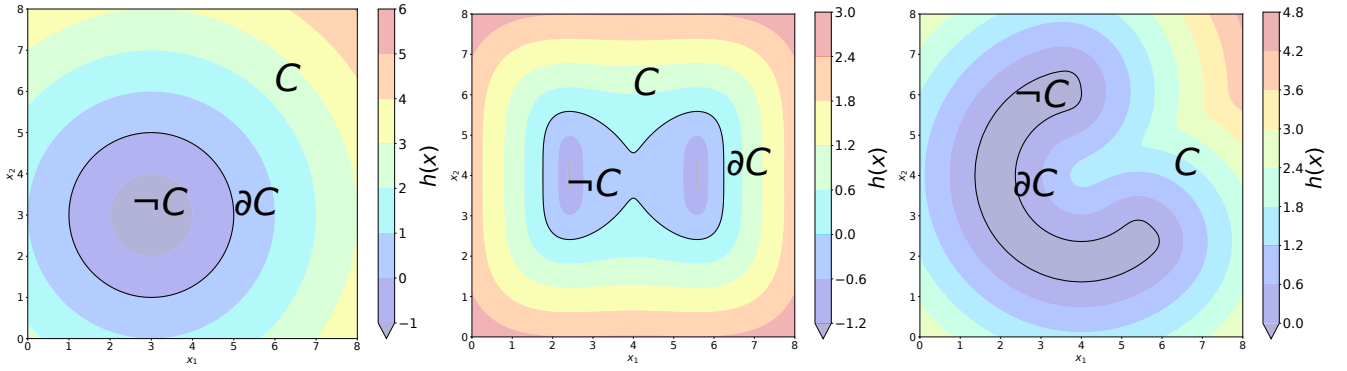


Fig. 1: Isolines displaying the value changes of h_{conv} , h_{star} , and h_{nstar} in the proximity of respectively a circle, a funnel and a C-shaped obstacle.

The hyperplane $H(x, t)$ is an orthonormal basis formed by basis vectors $e_1(x, t), \dots, e_{d-1}(x, t) \in \mathbb{R}^{d \times 1}$. The basis matrix $E(x, t)$ enforces the redistribution of velocities along $d(x, t), e_1(x, t), \dots, e_{d-1}(x, t)$. The magnitudes of the velocities in the redistributed directions are then modified by $D(x, t)$ as in Eq. (16). To achieve multiple obstacle avoidance, a weighted sum of the stretched velocity computed with respect to each obstacle is used, the details of which can be found in [11].

$$\begin{aligned} M(x, t) &= E(x, t)D(x, t)E(x, t)^{-1} \\ D(x, t) &= \text{diag}(\lambda(x, t), \lambda_e(x, t), \dots, \lambda_e(x, t)) \\ H(x, t) &= [e_1(x, t) \dots e_{d-1}(x, t)] \\ E(x, t) &= [d(x, t) \ H(x, t)] \end{aligned} \quad (16)$$

There exist 3 main variants of Mod-DS approaches, different in terms of how $E(x, t)$ and $D(x, t)$ are constructed: normal Mod-DS, reference Mod-DS and on-manifold Mod-DS [11][13][16]. The properties of each method are detailed in Table I. Since any smooth vector field in a sphere world has at least as many topologically critical points as obstacles [21], we consider a method to be able to handle certain types of obstacles if the modified DS has at most 1 local minimum per obstacle given a fully-actuated nominal DS. On any non-equilibrium points in the modified DS, Mod-DS approaches have been proven to ensure *impenetrability* at the boundary in the sense of von Neuman and if the nominal DS \dot{x}_{nom} is globally asymptotically stable (g.a.s) then Mod-DS is g.a.s. to the same equilibrium point $x^* \in \mathbb{R}^d$ [11, 16].

Normal Mod-DS: In normal Mod-DS, vector $n(x, t)$ normal to the boundary function $h(x, t)$ is used as the direction towards the obstacle when constructing the basis matrix $E(x, t)$ (17). It is noteworthy that $\lambda^*(x)$ and $\lambda_e^*(x)$ values listed in Table I are only popular choices of $D(x, t)$ but any $\lambda(x, t)$, $\lambda_e(x, t)$ satisfying conditions in (18) will be feasible options. As the earliest proposed Mod-DS variants, normal Mod-DS only guarantees convergence to target x^* in convex obstacle avoidance.

$$d_s(x, t) = n(x, t) = \frac{\nabla_x h(x, t)}{\|\nabla_x h(x, t)\|_2} \quad (17)$$

$$\lim_{h(x, t) \rightarrow 0} \lambda(x, t) = 0 \text{ and } \lambda_e(x, t) > 0 \ \forall x \in \mathbb{R}^d \quad (18)$$

Reference Mod-DS: The only difference between reference

Mod-DS and normal Mod-DS is that reference direction $r(x, t)$ is used instead of $n(x, t)$ to form the basis matrix $E(x, t)$ (19). $r(x, t)$ points from the agent's current location x to a reference point $r^*(t) \in \mathbb{R}^d$. r^* is a constant vector when the unsafe set is static. This change enables the reference Mod-DS to handle star-shaped obstacles, in addition to convex ones.

Definition 3.3 (Reference Points in Star-Shaped Obstacles) $r^*(t) \in \mathbb{R}^d$ is a reference point if and only if it is strictly inside unsafe set $-C$, where all rays from which have one and one only intersection with the boundary set ∂C . An obstacle or an unsafe set is considered star-shaped if it has a minimum of 1 reference point.

$$d_r(x, t) = r(x, t) = \frac{x - r^*(t)}{\|x - r^*(t)\|_2} \quad (19)$$

On-Manifold Mod-DS: On-manifold Mod-DS uses the same basis matrix $E(x, t)$ as the standard Mod-DS.

$$d_{\text{onM}}(x, t) = n(x, t) = \frac{\nabla_x h(x, t)}{\|\nabla_x h(x, t)\|_2} \quad (20)$$

However, unlike the other Mod-DS approaches that achieve safe control using uniform diagonal scaling policies defined in (18), on-manifold Mod-DS realizes undesirable-equilibrium-free safe control under the aggregate effects of 3 navigation policies, where λ_{∇} encodes the gradient descent dynamics, λ_{ϕ} enables on-manifold morphing dynamics and λ_h defines the regular Modulation dynamics.

$$\lambda(x, t) = \lambda_{\nabla}(x, t) + \lambda_{\phi}(x, t) + \varphi_h(x, t)\lambda_h(x, t) \quad (21)$$

The technical details of on-manifold Mod-DS can be found in [16]. In this work, we are more interested in the obstacle exit strategy $\phi(x, t)$ used in λ_{ϕ} to help efficiently circumnavigate both convex and concave unsafe regions. Let e^0 be one out of m candidate directions in \mathbb{R}^{d-1} , subject to $e^0 \notin \mathcal{N}(H(x, t))$, and $m \geq 2^{d-1}$. A geodesic approximation method can then utilize a first-order approximation to the obstacle surface to closely approximate a path $X = [x^0, x^1, \dots, x^N]$ exiting the obstacle on its isosurface, where horizon $N \in \mathbb{N}$ is a natural number [16]. Function $\phi(x, t) \in \mathbb{R}^d$ then outputs, among m candidate directions, the one with the smallest associated potential P_N , where β is the step size and $p(x)$ is a user-defined reward function. In most applications, $p(x)$ can be the distance from

Type	$D(x)$	$d(x, t)$	Obstacle	Local Minima #
Normal	$\lambda^*(x, t) = 1 - \frac{1}{h(x, t)+1}, \lambda_e^*(x, t) = 1 + \frac{1}{h(x, t)+1}$	$n(x, t)$	convex	1
Reference	$\lambda^*(x, t) = 1 - \frac{1}{h(x, t)+1}, \lambda_e^*(x, t) = 1 + \frac{1}{h(x, t)+1}$	$r(x, t)$	convex, star-shaped	1
On-Manifold	$D_{\nabla}(x, t) + D_{\phi}(x, t) + \varphi_h(x, t)D_h(x, t)$	$n(x, t)$	all	0

TABLE I: Properties of 3 main types of Mod-DS, including the definition of their basis matrix and diagonal scaling matrix, and the types of obstacles they can navigate without inducing a trapping region in the modified DS, are documented. For obstacle types that a Mod-DS variant can navigate without being trapped, the number of local minima that the approach induced per obstacle is listed. The definition of $n(x, t)$ and $r(x, t)$ can be found in Eq. (17) and (19)

x_i to the target x^* .

$$\begin{aligned}
 x^{i+1} &= \beta H(x^i, t) H(x^i, t)^\top e^i + x^i \\
 e^{i+1} &= \frac{H(x^i, t) H(x^i, t)^\top e^i}{\|H(x^i, t) H(x^i, t)^\top e^i\|_2} \\
 P_{i+1} &= P_i + \beta p(x^{i+1})
 \end{aligned} \tag{22}$$

IV. CBF-QP AND MOD-DS PERFORMANCE COMPARISON ON DIFFERENT OBSTACLE GEOMETRIES

In this section, we compare popular Mod-DS variants and CBF-QP with different α functions qualitatively and quantitatively in fully actuated systems. Since all existing Mod-DS approaches are developed based on fully actuated system assumptions, conclusions drawn in this section cannot be extended to control affine systems in general. Our analysis focuses on single-obstacle avoidance in static environment for ease of illustrative visualizations in Section IV-B and for comparable metrics in Section IV-C [11, 13, 14, 22, 6]. Characteristics of Mod-DS and CBF-QP approaches studied then contributes to the theoretical analysis in Section V.

A. Nominal Dynamics & Obstacle Definition

We define nominal controller u_{nom} to follow the integral curves of an autonomous linear 2D dynamical system (DS) as in (23), where $\epsilon \in \mathbb{R}^+$. This nominal DS is globally asymptotically stable at target $x^* = [0, 0]^\top$.

$$\dot{x}_{\text{nom}} = u_{\text{nom}} = -\epsilon x \quad \forall x \in \mathbb{R}^2 \tag{23}$$

Three obstacle geometries are explored in the comparison: i) a circle of radius 2 (4), ii) a star-shaped funnel centered at with $C_a = [2.5, 0]^\top$ and $c_b = 0.1$ (5), and iii) an open ring with an inner radius of 2 and an outer radius of 2.3.

B. Qualitative Comparison: Obstacle Geometry and Trapping Region

Mod-DS approaches' performances differ given their choices of $\lambda(x, t)$, $\lambda_e(x, t)$ and $d(x, t)$. Likewise, the parameterization of α functions CBF-QP affects the obstacle-avoiding behavior and speed profiles of the safe controller. In Figure 2 we present stream plots depicting the safe DS \dot{x} modified by CBF-QP and Mod-DS approaches respectively, given nominal DS in (23). Note that $\dot{x} = u$ in fully actuated systems (10).

1) *Preservation of Nominal DS*: By comparing the color, which indicates the magnitude of modified to nominal control output ratios, and curvature, which represents directions of the velocities u distorted by safe controllers at each state x , of the streamlines in Figure 2, it can be qualitatively concluded that CBF-QP with $\alpha(h) = h$ and Mod-DS's ability in preserving the nominal DS is weaker than CBF-QP with $\alpha(h) = 5h$, because streamlines or trajectories generated by CBF-QP with $\alpha(h) = 5h$ are straighter, i.e. more similar to that in nominal linear DS (23), and have larger yellow region. The color yellow means the magnitude of the modified controller $\|u\|_2$ is the same as that of the nominal ones $\|u_{\text{nom}}\|_2$ at that state x . In CBF-QP, the larger $\alpha(h)$ is, given input $h = h(x, t)$, the smaller the lower bound of $\dot{h}(x, t)$ is, which results in a larger feasible set for u . Mod-DS approaches are weaker in preserving the nominal DS than CBF-QP, which can be qualitatively observed from the coverage of red regions in Figure 2. Mod-DS modified controller often becomes larger in magnitude than the nominal controller because parameter λ_e (Table I) would boost \dot{x} in the directions tangent to the obstacles. Additionally, viewing from the streamlines' curvatures in row 7, on-manifold Mod-DS drastically alters and even reverses the directions of u_{nom} .

2) *Obstacle Geometries*: While CBF-QP and Mod-DS differ in their ability to preserve the nominal DS, they are similarly capable of handling convex obstacles. The generated trajectories form no obvious trapping regions, where the agent could be stuck, except an undesirable equilibrium at the boundary of the obstacle where u_{nom} and $\nabla_x h(x, t)$ are collinear. Further analysis of this undesirable equilibrium can be found in subsection IV-C. Plots 1(c)-5(c) and 1(e)-5(e) suggest the formation of a region of attraction when using CBF-QP to avoid star-shaped and non-star-shaped concave obstacles. Agents in the trapping region are led by one side of the obstacle boundary to move left and the other side to move right, which leads to convergence at an undesirable equilibrium point on the obstacle boundary. While the normal Mod-DS on row 5 forms the same trapping region as CBF-QP approaches, reference Mod-DS navigates star-shaped obstacles without forming any region of attraction and on-manifold Mod-DS is trapping-region-free for all obstacle geometries. Thus, the conclusion can be qualitatively drawn that reference and on-manifold Mod-DS provide more reasonable solutions facing concave obstacles.

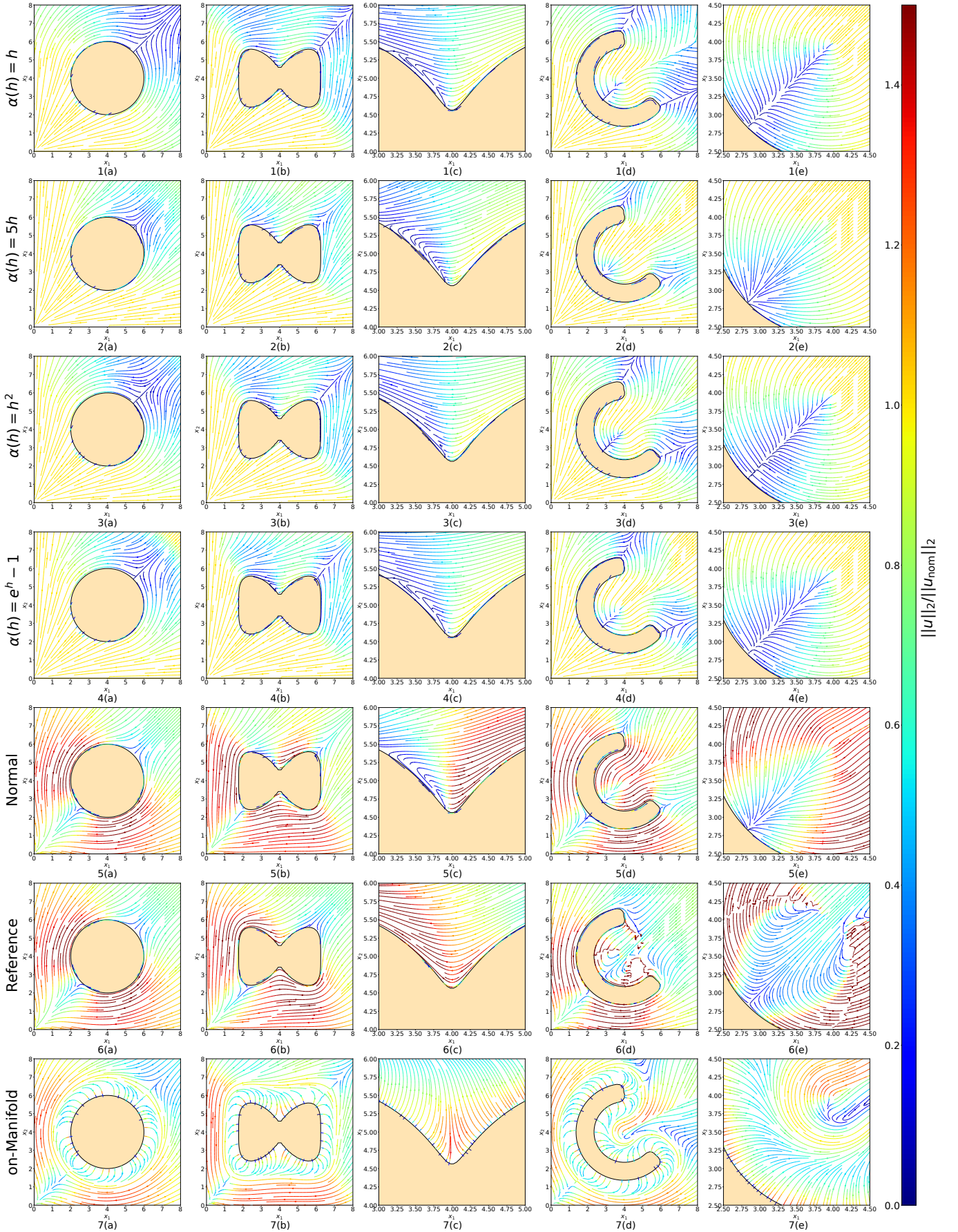


Fig. 2: Performance of different obstacle avoidance methods' facing respectively a convex, a star-shaped obstacle, and a non-star-shaped obstacle while following nominal linear DS in (23) with $\epsilon = 2$. First four columns (a)-(d) correspond to CBF-QP with different $\mathcal{K}_\infty \alpha(h)$ functions. The last 3 column corresponds to Mod-DS approaches. The colors on the trajectories indicate the ratio of the agent's modified speed to its nominal speed $\frac{\|u\|_2}{\|u_{nom}\|_2}$ as defined in Eq. (23).

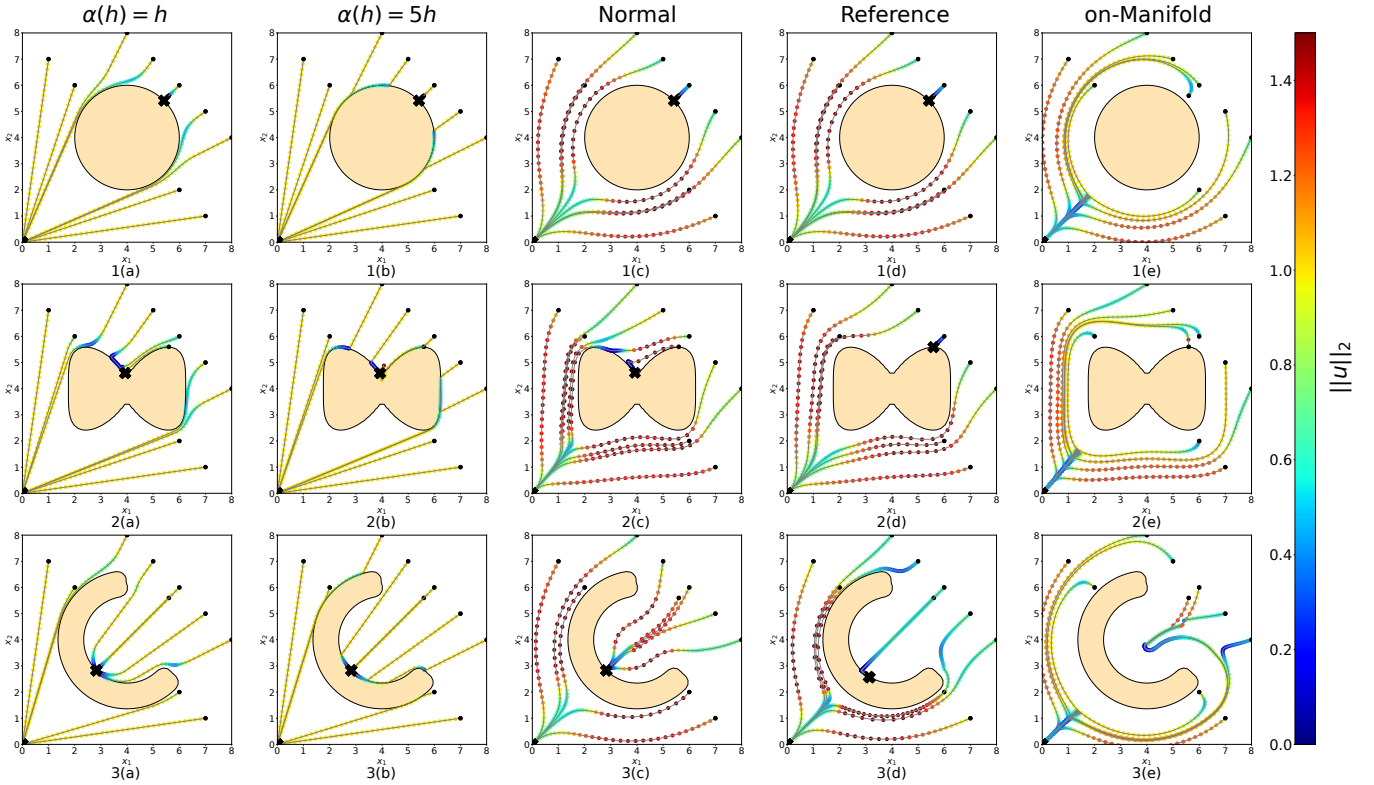


Fig. 3: Trajectories, with 10 initial locations and target at the origin, generated by Mod-DS and CBF-QP obstacle avoidance methods to avoid respectively a convex, a star-shaped obstacle, and a non-star-shaped obstacle given the nominal controller $\epsilon = \frac{1}{\|x\|_2}$ (23). First two columns correspond to CBF-QP with different \mathcal{K}_∞ $\alpha(h)$ functions. The last three columns correspond to Mod-DS approaches. The colors on the trajectories indicate the robot speed magnitude at that state x .

C. Quantitative Behavior Comparison

In addition to obstacle geometry and the ability to preserve nominal DS, we present quantitative analysis on the behavior metrics of CBF-QP and Mod-DS approaches in Table II.

Metrics: We utilized a set of controller behavior metrics proposed in [23], including trajectory length l , average weighted jerk \bar{j} , straight-line deviation η , obstacle clearance d_{obs} , and lastly, near obstacle velocity v_{near} to evaluate of how distinct (or similar) the real-time collision avoidance performance of CBF-QP and Mod-DS approaches are. Straight-line deviation η is designed to measure the extent to which the agent trajectory deviates from the nominal straight-line path. Average weighted jerk \bar{j} measures the abruptness of the path planned and indicates the smoothness of the final robot trajectory which impacts control feasibility. Finally, obstacle clearance d_{obs} measures the average distance to the closest obstacles, and near obstacle velocity v_{near} computes the average velocity during timesteps when the robot is near the obstacle boundaries. Metric equations are provided in Appendix V.

Behavior Analysis: Each method listed in Table II was implemented in Python and evaluated on 10 trajectories starting respectively at points $[1, 7]^\top$, $[7, 1]^\top$, $[2, 6]^\top$, $[6, 2]^\top$, $[4, 8]^\top$, $[8, 4]^\top$, $[5, 7]^\top$, $[7, 5]^\top$, $[5.6, 5.6]^\top$, $[6, 6]^\top$. The resulted 10 trajectories from each method can be found in Figure 3. Note that behavior metrics of length ratio l/l_{nom} , obstacle clearance d_{obs} and near obstacle velocity v_{near} in Table II are computed only using trajectories that have successfully

reached the target. The behavior metrics of weighted jerk \bar{j} and straight-line deviation η are computed using trajectories initiated at $[4, 8]^\top$ and $[7, 5]^\top$ (if succeeded in arriving at the target) because comparing \bar{j} and η across different trajectories results in unreasonably high standard deviation values. The 2 selected trajectories, interacting with regions closer to the obstacle than the rest, are good representations of each method's characteristics.

As reactive safe control methods, both Mod-DS and CBF-QP have quick runtime, making them useful in highly dynamic environments. Mod-DS approaches' strength is their high flexibility and adaptation to all obstacle geometries using different eigenvector and eigenvalue combinations. That ability enables Mod-DS variants like on-manifold Mod-DS to realize local minimum free obstacle avoidance, proven by its 100% success rate in converging to the target in Table II. Additionally, on-manifold Mod-DS has the highest obstacle clearance d_{obs} among all, indicating higher safety guarantees with less chance of collisions. on-manifold Mod-DS's drawback is slower runtime (though still fast enough to be reactive), the high demand for jerk j when reshaping the flow, longer trajectories l , and larger straight-line deviation η . On the contrary, CBF-QP methods are capable of generating smooth and efficient trajectories with low j and low v_{near} and low length ratios l/l_{nom} , while their weaknesses are small target reaching rate, which reveals the existence of numerous local minima in the CBF-QP modified trajectories. Normal Mod-DS's performance

Shape	Method	l/l_{nom} (std)	\bar{j} (std)	d_{obs} (std)	v_{near} (std)	η (std)	Runtime (s)	Success %
Convex	CBF-QP $\alpha = h$	1.03 (0.02)	1.32 (0.04)	2.43 (0.39)	0.96 (0.05)	0.34 (0.21)	0.0025	80
	CBF-QP $\alpha = 5h$	1.03 (0.03)	1.55 (0.03)	2.40 (0.41)	0.97 (0.04)	0.30 (0.22)	0.0026	80
	Normal Mod-DS	1.06 (0.03)	1.17 (0.04)	2.52 (0.41)	1.20 (0.02)	0.56 (0.07)	0.0002	80
	Reference Mod-DS	1.06 (0.03)	1.17 (0.04)	2.52 (0.41)	1.20 (0.02)	0.56 (0.07)	0.0002	80
	on-Mani Mod-DS	1.27 (0.17)	1.79 (0.71)	2.63 (0.34)	0.94 (0.10)	0.97 (0.13)	0.0004	100
Star	CBF-QP $\alpha = h$	1.03 (0.03)	1.55 (0.05)	2.39 (0.33)	0.95 (0.06)	0.49 (0.21)	0.0025	70
	CBF-QP $\alpha = 5h$	1.04 (0.04)	1.72 (0.06)	2.36 (0.35)	0.96 (0.06)	0.45 (0.21)	0.0025	70
	Normal Mod-DS	1.09 (0.07)	2.65 (0.68)	2.20 (0.40)	1.20 (0.07)	0.55 (0.07)	0.0002	90
	Reference Mod-DS	1.07 (0.05)	2.07 (0.68)	2.31 (0.37)	1.25 (0.04)	0.60 (0.04)	0.0002	80
	on-Mani Mod-DS	1.28 (0.17)	3.03 (1.16)	2.46 (0.26)	0.95 (0.12)	1.02 (0.09)	0.0005	100
Non-star	CBF-QP $\alpha = h$	1.02 (0.01)	1.31 (NA)	2.07 (0.24)	0.98 (0.03)	0.43 (NA)	0.0069	50
	CBF-QP $\alpha = 5h$	1.02 (0.02)	1.64 (NA)	2.06 (0.25)	0.99 (0.02)	0.39 (NA)	0.0057	50
	Normal Mod-DS	1.07 (0.03)	0.98 (NA)	2.13 (0.31)	1.30 (0.06)	0.64 (NA)	0.0065	50
	Reference Mod-DS	1.11 (0.06)	1.16 (0.08)	2.10 (0.28)	1.28 (0.06)	0.90 (0.25)	0.0055	80
	on-Mani Mod-DS	1.51 (0.34)	2.25 (0.44)	2.38 (0.15)	0.90 (0.10)	1.14 (0.04)	0.01224	100

TABLE II: Characteristics of trajectories generated using Mod-DS, and CBF-QP approaches in static obstacle avoidance at a controlled update frequency of 5Hz. The characteristics preferred by an ideal obstacle avoidance trajectory should contain small trajectory length l (or equivalently small trajectory length ratio l/l_{nom}), small average jerk \bar{j} , large obstacle clearance d_{obs} , small near obstacle velocities v_{near} , small straight line deviation η , low execution time and high success rate in converging to the goal location. Here, the methods that perform worst in a behavior evaluation category are colored red and those that perform best are colored green. For metrics computed only on a single trajectory because the rest failed in converging to the goal, their standard deviations are marked as "NA" (not applicable).

metrics are similar to that of the CBF-QP, except that the method's popular choice of eigenvalues $\lambda_e > 1$ (see Table I) results in higher robot velocities in the direction tangent to the boundary set ∂C and a larger chance for the robot to move away from local minima on concave obstacles' boundaries. Therefore, normal Mod-DS metrics have higher near-obstacle velocities v_{near} and slightly higher convergence rate than CBF-QPs. Lastly, Reference Mod-DS's behaviors are similar to normal Mod-DS in length ratio l/l_{nom} , obstacle clearance d_{obs} and near-obstacle velocity v_{near} . But the replacement of normal vector n with reference vector r gives reference Mod-DS a better convergence rate for non-convex obstacle avoidance.

Based on the above analysis, conclusions can be drawn that extended Mod-DS approaches of reference and on-manifold Mod-DSs are preferred to CBF-QP for obstacle avoidance in environments with concave obstacles using fully actuated systems. While CBF-QP-generated trajectories are more efficient, this efficiency has been shadowed by its low target-reaching rate.

V. THEORETICAL CONNECTIONS BEHIND MOD-DS AND CBF-QP IN FULLY-ACTUATED SYSTEMS

Qualitative and quantitative analysis of Mod-DS and CBF-QP approaches for fully actuated systems reveals some common features shared by the two seemingly distinctive approaches: given the same input state x , static obstacle environment $h(x)$ and nominal controller u_{nom} , normal Mod-DS shares the same local minimum set with CBF-QP. In this section, we demonstrate with mathematical derivations the theoretical connections responsible for similar behaviors in Mod-DS and CBF-QP performances. We prove that normal Mod-DS is equivalent to CBF-QP under certain choices of λ and λ_e in (16) and (18). We also show that solutions from reference Mod-DS are guaranteed to satisfy CBF conditions in (7) and the relationship between reference Mod-DS and CBF-

QP can be mathematically quantified to convert one from another. This conversion formula is important because it shows the key closed-form components in reference Mod-DS solutions that make possible navigation in star-shaped obstacle environments with few local minima. In section VII, through inverse engineering from the conversion formula, modifications of CBF-QP that enable concave unsafe set navigation with fewer and even no local minima are proposed. Note that in this section, our theoretical analysis focuses on static obstacle environment settings. Hence, $h(x)$, $n(x)$, and $r(x)$ are used instead of $h(x, t)$, $n(x, t)$, and $r(x, t)$ to represent boundary functions, normal vectors and reference vectors.

A. Local Minima in Mod-DS and CBF-QP

Local minima in Mod-DS are originated from inverse collinearity between the fully actuated nominal controller $\dot{x}_{\text{nom}} = u_{\text{nom}}$ and the gradient of the boundary function $\nabla_x h(x)$ (a.k.a the barrier function in CBF-QP formulations). In normal and reference Mod-DS, the modified controllers fail to converge to the target x^* when the nominal controller is inversely collinear with the normal direction $n(x)$ and the reference direction $r(x)$ respectively [Definition 5.1, 5.2].

Definition 5.1 (Saddle Equilibria in Normal Mod-DS) *When normal Mod-DS constantly encounters inverse collinearity between \dot{x}_{nom} and $n(x)$; i.e., $\langle \frac{\dot{x}_{\text{nom}}}{\|\dot{x}_{\text{nom}}\|}, n(x) \rangle = -1$, the subsequent solutions of Eq. (14), (16), (17) will lead the agent to an undesirable equilibrium, $\dot{x} = u_{\text{mod}} \rightarrow \mathbf{0}$, on the boundary of the obstacle ∂C [11].*

Definition 5.2 (Saddle Equilibria in Reference Mod-DS) *When reference Mod-DS constantly encounters inverse collinearity between \dot{x}_{nom} and $r(x)$; i.e., $\langle \frac{\dot{x}_{\text{nom}}}{\|\dot{x}_{\text{nom}}\|}, r(x) \rangle = -1$, the subsequent solutions of Eq. (14), (16), (19) will lead the agent to an undesirable equilibrium, $\dot{x} = u_{\text{mod}} \rightarrow \mathbf{0}$, on the boundary of the obstacle ∂C [13].*

Interestingly, very few works have discussed undesirable local minimum (or undesirable equilibrium) issues in CBF-QPs. In [22], this limitation of CBF-QPs was identified. However, they did not offer rigorous proof for the existence of such saddle points, only a solution to alleviate them. [24] explored the issue for Control Lyapunov Function and Control Barrier Function-based Quadratic Programs (CLF-CBF-QPs), where they showed that even for convex obstacle shapes undesirable equilibria can be introduced on the boundaries due to the contradictions between CLF and CBF constraints. Following, we offer formal proof showing that, in fully actuated systems, undesirable equilibria in CBF-QP can also originate from inverse collinearity, the same as that in normal Mod-DS.

Theorem 5.3 (Saddle Equilibria in CBF-QP) *When a fully-actuated CBF-QP controller constantly encounters inverse collinearity between $\nabla_x h(x)$ and u_{nom} ; i.e., $\langle n(x), \frac{u_{\text{nom}}}{\|u_{\text{nom}}\|} \rangle = -1$, the subsequent solutions of Eq. (11), or equivalently Eq. (13), will lead the agent to an undesirable equilibrium, $\dot{x} = u_{\text{mod}} \rightarrow \mathbf{0}$, at the boundary of the obstacle ∂C .*

Proof: Since $\nabla_x h(x)$ and u_{nom} are inversely collinear with each other, there exist a constant scalar $c \in \mathbb{R}^-$ s.t. $u_{\text{nom}} = c\nabla_x h(x)$. Denote $\nabla_x h = \nabla_x h(x)$ and $\alpha = \alpha(h(x))$. Equation 13 can then be rewritten as

$$u_{\text{cbf}} = \begin{cases} c\nabla_x h & \text{if } \|\nabla_x h\|_2^2 \leq -\frac{\alpha}{c} \\ c\nabla_x h - \frac{c\nabla_x h^\top \nabla_x h + \alpha}{\nabla_x h^\top \nabla_x h} \nabla_x h & \text{otherwise} \end{cases} \quad (24)$$

$$= \begin{cases} c\nabla_x h & \text{if } \|\nabla_x h\|_2^2 \leq -\frac{\alpha}{c} \\ -\frac{\alpha}{\|\nabla_x h\|_2^2} \nabla_x h & \text{otherwise} \end{cases}.$$

Given any initial state $x^0 \in C$, if $\|\nabla_x h(x^0)\|_2^2 \leq -\frac{\alpha(h(x^0))}{c}$, $u_{\text{cbf}} = c\nabla_x h(x^0)$. Since $c < 0$, this command moves the agent in the direction opposite to the gradient of the boundary function $h(x^i)$ and makes the value of $h(x^i)$ decrease in the subsequent timesteps $i \in \{1, 2, \dots\}$. If $\nabla_x h(x^i)$ stays constantly inversely collinear with u_{nom} , $\alpha(h(x^i))$ value would decrease until $\|\nabla_x h(x^i)\|_2^2 > -\frac{\alpha(h(x^i))}{c}$. When $u_{\text{cbf}} = -\frac{\alpha(h(x^i))}{\|\nabla_x h(x^i)\|_2^2} \nabla_x h(x^i)$, the agent is still commanded to move in the direction opposite to the gradient of the boundary function $h(x^i)$, despite with a slower speed. Similarly, $\alpha(x^i)$ value will keep decreasing until it reaches 0 at the boundary set ∂C if inverse collinearity persists.

$$\lim_{\alpha \rightarrow 0} u_{\text{cbf}} = \lim_{\alpha \rightarrow 0} -\frac{\alpha}{\|\nabla_x h\|_2^2} \nabla_x h = \mathbf{0} \quad (25)$$

Therefore, when CBF-QP with fully-actuated systems encounters inverse collinearity constantly between u_{nom} and $\nabla_x h(x)$, the subsequent solutions lead the agent to an undesirable equilibrium. ■

B. Normal Mod-DS and CBF-QP Equivalence

The similarity between CBF-QP and Mod-DS in terms of undesirable equilibria originated from the fact that the normal Mod-DS approach is equivalent to CBF-QP.

Theorem 5.4 (Normal Mod-DS and CBF-QP Equivalence) *When the unsafe set is static, given fully-actuated CBF-QP*

controllers with any choice of extended K_∞ function α , there exists a pair of λ and λ_e such that normal Mod-DS defined in Eq. (14), (18) and (17) perform equivalently.

Proof: In static environments, orthonormal basis $E(x) = [\frac{\nabla_x h(x)}{\|\nabla_x h(x)\|_2}, H(x)]$ in (16) defines an obstacle-based coordinate system different from the world frame. To simplify the derivation expressions, we again abuse notations and let $\alpha = \alpha(h(x))$, $\nabla_x h = \nabla_x h(x)$, $H = H(x)$, $E = E(x)$ and $M = M(x)$. Since E is orthonormal, $E^{-1} = E^\top = [\frac{\nabla_x h}{\|\nabla_x h\|_2}^\top; H^\top]$. $H^\top \nabla_x h = \mathbf{0}_{(d-1) \times 1}$. Projecting the solution in (13) from the world frame to the obstacle-based coordinate frame defined by E , we get the following expressions.

$$E^{-1}u_{\text{cbf}} = E^\top u_{\text{cbf}} = \begin{bmatrix} \frac{\nabla_x h^\top}{\|\nabla_x h\|_2} \\ H^\top \end{bmatrix} u_{\text{cbf}}$$

$$= \begin{cases} \begin{bmatrix} \frac{\nabla_x h^\top}{\|\nabla_x h\|_2} \\ H^\top \end{bmatrix} u_{\text{nom}} & \text{if } \nabla_x h^\top u_{\text{nom}} \geq -\alpha \\ \begin{bmatrix} \frac{\nabla_x h^\top}{\|\nabla_x h\|_2} \\ H^\top \end{bmatrix} u_{\text{nom}} - \begin{bmatrix} \frac{\nabla_x h^\top u_{\text{nom}} + \alpha}{\|\nabla_x h\|_2} \\ \mathbf{0}_{(d-1) \times d} \end{bmatrix} & \text{otherwise} \end{cases} \quad (26)$$

$$= \begin{cases} \begin{bmatrix} \frac{\nabla_x h^\top}{\|\nabla_x h\|_2} \\ H^\top \end{bmatrix} u_{\text{nom}} & \text{if } \nabla_x h^\top u_{\text{nom}} \geq -\alpha \\ \begin{bmatrix} -\alpha \\ \frac{\nabla_x h^\top u_{\text{nom}}}{H^\top} \end{bmatrix} & \text{otherwise} \end{cases}$$

Similarly, projecting the solution from Eq. (14), (16), (17) into the coordinate system defined by E , the following relationship can be acquired between λ , λ_e value and $E^{-1}u_{\text{mod}}$. Note that $\dot{x}_o = 0$ when the obstacle is static.

$$E^{-1}u_{\text{mod}} = E^{-1}Mu_{\text{nom}} = DE^\top u_{\text{nom}}$$

$$= \begin{bmatrix} \lambda \frac{\nabla_x h^\top}{\|\nabla_x h\|_2} \\ \lambda_e H^\top \end{bmatrix} u_{\text{nom}} \quad (27)$$

Select λ and λ_e as shown in (28). Since $\alpha = \alpha(h(x)) \rightarrow 0$ as $h(x) \rightarrow 0$ due to the property of K_∞ functions. Therefore, λ and λ_e trivially satisfy the requirement in (18).

$$\lambda = \begin{cases} 1 & \text{if } \nabla_x h^\top u_{\text{nom}} \geq -\alpha \\ -\frac{\alpha}{\nabla_x h^\top u_{\text{nom}}} & \text{otherwise} \end{cases} \quad \lambda_e = 1 \quad (28)$$

Plug (28) into (27), we get

$$E^{-1}u_{\text{mod}} = \begin{cases} \begin{bmatrix} \frac{\nabla_x h^\top}{\|\nabla_x h\|_2} \\ H^\top \end{bmatrix} u_{\text{nom}} & \text{if } \nabla_x h^\top u_{\text{nom}} \geq -\alpha \\ \begin{bmatrix} -\alpha \\ \frac{\nabla_x h^\top u_{\text{nom}}}{H^\top} \end{bmatrix} & \text{otherwise} \end{cases}$$

$$= E^{-1}u_{\text{cbf}}. \quad (29)$$

If a pair of vectors is equivalent when measured in one coordinate system, they must also be equivalent in all coordinate systems. Therefore, the conclusion can be drawn that $u_{\text{cbf}} = u_{\text{mod}}$ when λ and λ_e are defined as in (28). ■

To further validate our theorem, given nominal DS defined in (23), the modified DSs produced respectively by normal Mod-DS, satisfying (28) and by CBF-QP with $\alpha(h) = h$

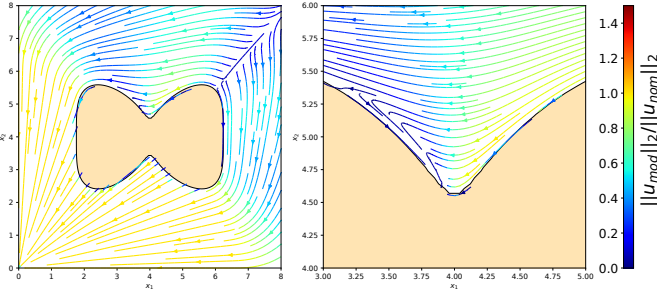


Fig. 4: Performance of the normal Mod-DS given λ, λ_e in (28) is equivalent to that of CBF-QP with $\alpha(h) = h$ in Figure 2.

are presented in Figure 4. The magnitude (represented by the color of the streamlines) and direction (represented by streamline directions) of normal Mod-DS modified DS in Figure 4 are exactly the same as those in the corresponding CBF-QP modified DS in Figure 2 1(b) and 1(c).

C. Reference Mod-DS and CBF-QP Similarities

In subsection IV-B, the performance of the reference Mod-DS was demonstrated to be superior to that of the CBF-QP. Still, the fact that reference Mod-DS shared the same undesirable local minimum with CBF-QPs for circular obstacle avoidance in Figure 3 suggests the potential for hidden connections between the 2 seemingly distinctive approaches. Quantifying the similarities and differences between reference Mod-DS and CBF-QP is key to understanding how undesirable local minima can be reduced or even eliminated to realize global convergence. We begin our discussion here by proving u_{mod} from reference Mod-DS satisfies the CBF constraints at all times and then quantify what changes need to be introduced before reference Mod-DS and CBF-QP can be converted to each other. The theoretical connections discussed here will contribute to the design of a new safe control approach that incorporates the advantage of reference Mod-DS and CBF-QP in section VII.

Theorem 5.5 (Safe Set Invariance in Reference Mod-DS)

Given fully-actuated nominal controller u_{nom} in (10) and any λ and λ_e satisfying (18), there exists an extended class K_∞ function such that the Mod-DS safe controller u_{mod} defined in Eq. (14), (16), and (19) meets the CBF conditions defined in Eq. (11).

Proof: Since we assume that the unsafe sets are translating and rotating rather than expanding, there must exist a point x_o somewhere such that the motion of an unsafe set can be characterized about. Thus, $\frac{\partial h(x,t)}{\partial t}$ can be rewritten as in (30), where \dot{x}_o can be computed as in (15).

$$\begin{aligned} \frac{\partial h(x,t)}{\partial t} &= \frac{\partial h(x-x_o(t))}{\partial t} = \nabla_{x_o} h(x-x_o(t))^\top \dot{x}_o \\ &= -\nabla_x h(x-x_o(t))^\top \dot{x}_o \\ &= -\nabla_x h(x,t)^\top \dot{x}_o. \end{aligned} \quad (30)$$

Plug (30) into the CBF constraint in (11), CBF conditions in fully actuated systems are equivalent to the following. Denote

$$h(x,t) = h \text{ and } \nabla_x h = \nabla_x h(x,t).$$

$$\frac{\nabla_x h^\top}{\|\nabla_x h\|_2} u \geq \frac{\nabla_x h^\top}{\|\nabla_x h\|_2} \dot{x}_o - \frac{\alpha(h)}{\|\nabla_x h\|_2} \quad (31)$$

Following the same notation as in Theorem 5.4, $\forall x \in \mathbb{R}^d$, denote $H = [e_1(x,t), \dots, e_{d-1}(x,t)] \in \mathbb{R}^{d \times (d-1)}$ to be the hyperplane perpendicular to the gradient of the boundary function $\nabla_x h$. Denote $r = r(x,t)$, $e_i = e_i(x,t)$, $i \in \{1, 2, \dots, d-1\}$ and the basis matrix of reference Mod-DS $E_r = [r(x,t), H(x,t)]$, as defined in (16) and (19). Note that $\|r(x,t)\|_2 = 1$ by definition. Note that since $E_r r(x,t)$ is an orthonormal basis, $E_r^{-1} \neq E_r^\top$. Instead,

$$\begin{aligned} E_r^{-1} &= \begin{bmatrix} \frac{1}{\nabla_x h^\top r} \nabla_x h^\top \\ -\frac{1}{\nabla_x h^\top r} e_1^\top r \nabla_x h^\top + e_1^\top \\ \vdots \\ -\frac{1}{\nabla_x h^\top r} e_{d-1}^\top r \nabla_x h^\top + e_{d-1}^\top \end{bmatrix} \\ &= \begin{bmatrix} \frac{1}{\nabla_x h^\top r} \nabla_x h^\top \\ H^\top (I - \frac{1}{\nabla_x h^\top r} r \nabla_x h^\top) \end{bmatrix}. \end{aligned} \quad (32)$$

Therefore, the decomposition of u_{mod} onto $r(x,t)$ by basis matrix E_r can be computed from Eq. (14) and (16) as

$$\begin{aligned} u_{\text{mod}}^r &= \lambda E_r^{-1} [1, :](u_{\text{nom}} - \dot{x}_o) + E_r^{-1} [1, :]\dot{x}_o \\ &= \frac{\lambda}{\nabla_x h^\top r} \nabla_x h^\top u_{\text{nom}} + \frac{1-\lambda}{\nabla_x h^\top r} \nabla_x h^\top \dot{x}_o \\ &= \frac{\nabla_x h^\top}{\nabla_x h^\top r} [\lambda u_{\text{nom}} + (1-\lambda)\dot{x}_o]. \end{aligned} \quad (33)$$

The decomposition of u_{mod} onto $r(x,t)$ can be further broken down in direction $n(x,t)$ parallel to $\nabla_x h$ and direction $e = e(x,t)$ on the tangent hyperplane $H(x,t)$. The projection of u_{mod} onto $n(x,t)$ is equivalent to the projection of u_{mod} first onto $r(x,t)$ and then onto n , i.e. the projection of $u_{\text{mod}}^r r(x,t)$ onto $n(x,t)$, because the vector $e(x,t)$ is orthogonal to $n(x,t)$, i.e. $\langle n(x,t), e(x,t) \rangle = 0$.

$$\begin{aligned} u_{\text{mod}}^n &= n^\top (u_{\text{mod}}^r r + u_{\text{mod}}^H e) = n^\top u_{\text{mod}}^r r \\ &= n^\top r \left\{ \frac{\nabla_x h^\top}{\nabla_x h^\top r} [\lambda u_{\text{nom}} + (1-\lambda)\dot{x}_o] \right\} \end{aligned} \quad (34)$$

From the relationship between vector $n(x,t)$ and $r(x,t)$ depicted in Figure 5b, it can be deduced that

$$\langle \hat{n}, \hat{r} \rangle = \frac{\nabla_x h^\top}{\|\nabla_x h\|_2} r = \cos \theta. \quad (35)$$

Since $-\pi/2 \leq \theta \leq \pi/2$ under all conditions because the reference direction $r(x,t)$ and the normal direction $n(x,t)$ must both point away from the obstacle, $\cos \theta \geq 0$ always holds. Therefore, plugging (35) into (34),

$$\begin{aligned} u_{\text{mod}}^n &= \cos \theta \left\{ \frac{\nabla_x h^\top}{\nabla_x h^\top r} [\lambda u_{\text{nom}} + (1-\lambda)\dot{x}_o] \right\} \\ &= \frac{\nabla_x h^\top}{\|\nabla_x h\|_2} [\lambda u_{\text{nom}} + (1-\lambda)\dot{x}_o]. \end{aligned} \quad (36)$$

Now we are left with showing the modulated value in (34) satisfies the CBF condition in (11). WTS: \forall possible $\nabla_x h(x,t)$, $h(x,t)$, u_{nom} , \dot{x}_o and λ combinations, there exists a

K_∞ function α such that the following inequality, acquired by plugging $\frac{\nabla_x h^\top}{\|\nabla_x h\|_2} u = u_{\text{mod}}^n$ from (36) into (31) and simplify, always holds.

$$\alpha(h) \geq -\lambda \nabla_x h^\top u_{\text{nom}} + \lambda \nabla_x h^\top \dot{x}_o \quad (37)$$

Since the norms of $\nabla_x h(x, t)$, $h(x, t)$, u_{nom} , \dot{x}_o and λ values are all well-bounded in real-life robot applications, find α that serve as an upper bound for domain $\{x \in \mathbb{R}^d : h(x, t) > 0\}$ is trivial. When $h(x, t) = 0$, $\lambda = 0$ based on (18), the left and right sides of the inequality become 0 and satisfy the property of K_∞ functions. In conclusion, given a bounded fully-actuated nominal controller u_{nom} in (10) and any feasible λ and λ_e , there exists an extended class K_∞ function such that the Mod-DS safety controller u_{mod} meets the CBF conditions. ■

Theorem 5.6 (Quantitative Difference between Reference Mod-DS and CBF-QP) *Given any CBF-QP with a fully-actuated nominal controller u_{nom} in (10), there exist a pair of λ , λ_e values satisfying (18) such that the differences between outputs from reference Mod-DS and CBF-QP can be quantified as $(\lambda_e - \lambda) \sum_{i=1}^{d-1} \frac{e_i^\top r}{n^\top r} e_i n^\top u_{\text{nom}}$. In the expression, we abuse notation and let $r = r(x, t)$ in (19), $e_i = e_i(x, t)$ in (16) and $n = n(x, t)$ in (17).*

Proof: Since both normal and reference Mod-DS are reactive safe control approaches with explicit closed-form solutions, given the same λ and λ_e , the differences between reference and normal Mod-DS in regions where both are active can be computed as in [16]. Here to distinguish reference Mod-DS outputs from the normal ones, we denote results from reference Mod-DS as u_{mod}^R and that from the normal one as u_{mod}^N .

$$u_{\text{mod}}^R = u_{\text{mod}}^N - (\lambda_e - \lambda) \sum_{i=1}^{d-1} \frac{e_i^\top r}{n^\top r} e_i n^\top u_{\text{nom}} \quad (38)$$

Because CBF-QP is demonstrated to be equivalent to normal Mod-DS in Theorem 5.4, setting reference Mod-DS to be only active in scenarios where CBF-QP is, i.e. $u_{\text{mod}}^R = u_{\text{nom}}$ when $\nabla_x h^\top u_{\text{nom}} \geq -\alpha$ similar to (13), it can be trivially concluded that,

$$u_{\text{mod}}^R - u_{\text{cbf}} = \begin{cases} 0 & \text{if } \nabla_x h^\top u_{\text{nom}} \geq 0 \\ -(\lambda_e - \lambda) \sum_{i=1}^{d-1} \frac{e_i^\top r}{n^\top r} e_i n^\top u_{\text{nom}} & \text{otherwise} \end{cases} \quad (39)$$

Here ends our comparative analysis of the connections and differences between Mod-DS and CBF-QP methods. Given conclusions made in section IV, we propose speed and velocity constraining Mod-DS to boost reference Mod-DS and on-manifold Mod-DS's advantage over CBF-QP in concave-obstacle environments. The new feature will allow Mod-DS to have abilities comparable with CBF-QP in enforcing kinematic constraints in fully actuated systems. ■

VI. CONSTRAINED MOD-DS IN FULLY-ACTUATED SYSTEMS

In section IV, Mod-DS's strength in navigating around a larger variety of obstacles with fewer undesirable local

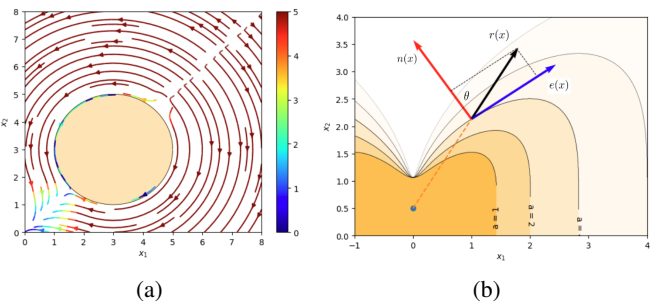


Fig. 5: Figure 5a shows the performance of speed-constraining (5 units/s) reference Mod-DS from [25]. Notice the excessive 90-degree sharp turns. Figure 5b illustrates the geometric interpretation and relationship between $n(x)$, $e(x)$ and $r(x)$ used for Theorem 5.5.

minima is demonstrated, which makes it a more suitable option for robots with fully actuated systems. However, some may argue that all Mod-DS approaches have limitations in handling input constraints. For closed-form methods in general, implementing velocity constraints poses challenges as modifications to the modulated velocity might compromise the agent's guaranteed impenetrability. A closed-form speed-constraining method was proposed for Mod-DS approaches in [25]. However, such methods are conservative, depriving the constrained trajectories of Mod-DS characteristics and generating sharp turns impractical for robots to follow in real life Figure 5a.

Here in this section, by posing Mod-DS's input constraining process as an independent convex optimization problem and proving mathematically that such optimization problem either has simple closed-form solutions or can be solved sufficiently fast, we argue that Mod-DS's constraints enforcement ability in fully-actuated systems is equivalent to that of CBF-QP. In robot applications, inputs constraints typically can be categorized into 2 types: speed constraints $\|\dot{x}\|_2 = \|u\|_2 \leq u_{\text{ub}}$, and velocity or box constraints $U_{\text{lb}} \leq u \leq U_{\text{ub}}$, where $u_{\text{ub}} \in \mathbb{R}$ and $U_{\text{lb}}, U_{\text{ub}} \in \mathbb{R}^d$. Following, one optimization problem is constructed for each constraint type. We again abused notation here and set $n = n(x, t)$, which is defined in (17).

A. Speed-Constraining Mod-DS

When the unconstrained output from Mod-DS $u_{\text{unc}} = \dot{x}_{\text{unc}}$ exceeds the speed limit, solving the following Quadratically Constrained Linear Programming (QCLP) problem finds the constrained output u_c that is most similar to u_{unc} and ensures safety (42) while satisfying speed input constraint u_{ub} (41). In both speed-constraining and velocity-constraining Mod-DS, robot safety is ensured by restricting the robot's velocity moving towards the obstacle, i.e. the projection of u_c onto vector $n(x, t)$, to be no larger than that of u_{unc} .

$$u_c = \arg \max_u \langle u_{\text{unc}}, u \rangle \quad (40)$$

$$\|u\|_2 \leq u_{\text{ub}} \quad (41)$$

$$\langle n, u \rangle \geq \min(\langle n, \dot{x}_o \rangle, \langle n, u_{\text{unc}} \rangle) \quad (42)$$

In speed-constraining Mod-DS, we make the design choice to measure similarity between the constrained and unconstrained Mod-DS outputs using dot products between the two vectors so that the QP has simple closed-form solutions. Using dot products as cost functions is reasonable because $\langle u_{\text{unc}}, u \rangle = \|u_{\text{unc}}\|_2 \|u\|_2 \cos \theta_d$, where $\theta_d \in [0, \pi]$ is the angle difference between the 2 vectors. $\|u_{\text{unc}}\|_2$ is fixed because u_{unc} is a constant vector input into the QP. When $\|u\|_2$ is also fixed, the dot product between u_{unc} and u is inversely correlated to θ_d . In other words, the larger the dot product is, the more similar u is to u_{unc} orientation-wise. We know the magnitude of the optimal solution of the QP u_c must be fixed to $\|u_c\|_2 = u_{\text{ub}}$, because the above optimization problem would only be called to modify u_{unc} when $\|u_{\text{unc}}\|_2 > u_{\text{ub}}$. Therefore, the optimization problem can be reformulated as the following. Note that $\langle a, b \rangle = a^\top b$ when $a, b \in \mathbb{R}^d$ and $\|u\|_2^2 = u^\top u$.

$$\begin{aligned} u_c &= \arg \max_u u_{\text{unc}}^\top u & (43) \\ u^\top u &= (u_{\text{ub}})^2 \\ n^\top u &\geq \min(n^\top \dot{x}_o, n^\top u_{\text{unc}}) \end{aligned}$$

Denote $v_n = \min(n^\top \dot{x}_o, n^\top u_{\text{unc}})$. Solving for the explicit solutions of the above convex optimization problem using Karush–Kuhn–Tucker (KKT) conditions, a simple explicit solution is found as in (44), where $v_e = \sqrt{\|u_{\text{unc}}\|_2^2 - \|n^\top u_{\text{unc}}\|_2^2} = \|H^\top u_{\text{unc}}\|_2$ is the projection of u_{unc} onto the hyperplane $H = H(x, t)$ tangent to the boundary function $h(x, t)$ (16).

$$\begin{cases} \frac{u_{\text{ub}}}{\|u_{\text{unc}}\|_2} u_{\text{unc}} & \text{if } \frac{u_{\text{ub}}}{\|u_{\text{unc}}\|_2} n^\top u_{\text{unc}} \geq v_n \\ v_n n + \frac{\sqrt{(u_{\text{ub}})^2 - (v_n)^2}}{v_e} (u_{\text{unc}} - u_{\text{unc}}^\top n n) & \text{otherwise} \end{cases} \quad (44)$$

The difference between the proposed method with the strategy in [25] is that ours considers the unconstrained Mod-DS outputs $n^\top u_{\text{unc}}$ when determining whether the robot is safe, which improves the smoothness of the trajectories generated by the constrained outputs and maximumly preserves the Mod-DS characteristics (see Figure 6).

B. Velocity-Constraining Mod-DS

Similarly, solving optimization problem in Eq. (45) offers solutions to enforcing velocity constraints $U_{\text{lb}} \leq u \leq U_{\text{ub}}$ for Mod-DS in fully-actuated systems while guaranteeing safety.

$$\begin{aligned} u_c &= \arg \min_u \|u - u_{\text{unc}}\|_2^2 & (45) \\ U_{\text{lb}} &\leq u \leq U_{\text{ub}} \\ n^\top u &\geq \min(n^\top \dot{x}_o, n^\top u_{\text{unc}}) \end{aligned}$$

Unlike the speed-constraining Mod-DS, the QP problem for enforcing velocity constraints no longer has a straightforward explicit solution, because the complexity of the explicit solution derived from KKT conditions grows exponentially with the number of inequality constraints in the problem. Note that both speed-constraining and velocity-constraining Mod-DS methods proposed here remain valid for high dimensional state-spaces when $d > 3$.

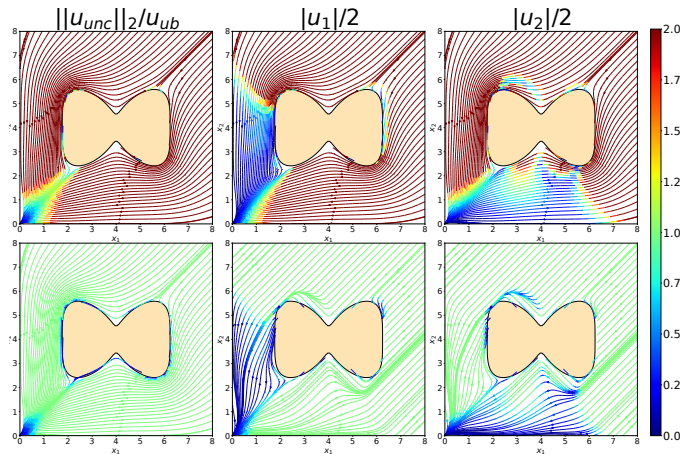


Fig. 6: Unconstrained reference Mod-DS (first row) vs. speed-constrained (second row, left) and velocity-constrained reference Mod-DS with $U_{\text{ub}} = -U_{\text{lb}} = [2, 2]^\top$ (second row, middle and right). The color codes for images in the left, middle, and right columns respectively represent $\frac{\|u_{\text{unc}}\|_2}{u_{\text{ub}}}$, $\frac{|u_1|}{2}$, and $\frac{|u_2|}{2}$, given that $u = [u_1, u_2]^\top$.

C. Theoretical Guarantees

Both speed and velocity constraining Mod-DS preserve the *impenetrability* guarantees of the original Mod-DS, under the assumption that the speed that the obstacle travels towards the agent is no more than the speed limit. We showcase stream plots in Figure 6 to demonstrate performances of speed-constraining and velocity-constraining Mod-DS compared to unconstrained Mod-DS.

Theorem 6.1: Consider an obstacle whose boundary is defined as $h(x, t) = 0$. Any trajectory $x(t)$, $t \in [0, \infty)$ starting outside the obstacle boundary, i.e., $h(x(0), 0) \geq 0$, evolving according to Eq. (14) and being constrained by the Speed-Constraining and Velocity-Constraining approaches Mod-DS presented in Section VI-A and VI-B, will never penetrate the obstacle boundary, i.e., $h(x(t), t) \geq 0, \forall t \in [0, \infty)$.

Proof: See Appendix B. ■

VII. MODULATION-BASED CONTROL BARRIER FUNCTIONS (MCBF)

In fully actuated systems, Mod-DS approaches outperform CBF-QP in navigating around non-convex unsafe sets with far fewer undesirable local minima. However, CBF-QP is still more commonly used in robot applications because it works for control affine systems in general and the QP formulations are more intuitive to the users. Nevertheless, choosing between superiority in handling complex robot dynamics and navigating among concave unsafe sets free of undesirable local minima should not be a tradeoff that users have to make when designing robot controllers. In this section, 2 Mod-based CBF-QP (MCBF-QP) approaches that combine the strength of CBF-QP with Mod-DS are proposed to ensure respectively few-local-minimum and local-minimum-free navigation in concave-obstacle environments with the ease of incorporating different robot dynamics.

A. Reference MCBF for Star-shaped Obstacle Avoidance

In subsection V-C, theoretical analysis of reference Mod-DS and CBF-QP demonstrated that CBF-QP's performance in $n(x, t)$ direction is similar to that of the reference Mod-DS in **Theorem 5.5**. Besides, in **Theorem 5.6**, reference Mod-DS's introduction of off-diagonal components in the tangent hyperplane $H(x, t)$ navigation is identified to be the major differences between CBF-QP and reference Mod-DS in fully-actuated systems and the key factor for reducing undesirable equilibrium in star-shaped obstacle avoidance. Adding additional constraints for u_{cbf} on the tangent hyperplane will reduce undesirable equilibrium caused by CBF constraints. In theory, there are numerous ways to incorporate the off-diagonal components into CBF-QP results. Here, we propose a linear constraint formulation that is mathematically simple and does not increase the complexity of the original CBF-QP problem. Note that $E_r(x, t)^{-1}[2 : d, :] \dot{x} = H(x, t)^\top (I - \frac{1}{\nabla_x h(x, t)^\top r} r \nabla_x h(x, t)^\top) \dot{x}$ solves for the projection of \dot{x} onto hyperplane $H(x, t)$ in basis $E_r(x, t)$. $g(x)$ and $E_r(x, t)^{-1}$ are defined in (8) and (32).

$$u_{\text{mcbf}} = \arg \min_{u \in \mathbb{R}^p, \rho \in \mathbb{R}^{d-1}} (u - u_{\text{nom}})^\top (u - u_{\text{nom}}) + \rho^\top \rho$$

$$L_f h(x, t) + L_g h(x, t) u + \frac{\partial h(x, t)}{\partial t} \geq -\alpha(h(x, t)) \quad (46)$$

$$H(x, t)^\top (I - \frac{r(x, t) \nabla_x h(x, t)^\top}{\nabla_x h(x, t)^\top r(x, t)}) g(x) (u - u_{\text{nom}}) = \rho \quad (47)$$

For fully-actuated systems in (10), the special case of MCBF-QP can be simplified as in (48).

$$u_{\text{mcbf}} = \arg \min_{u \in \mathbb{R}^d, \rho \in \mathbb{R}^{d-1}} (u - u_{\text{nom}})^\top (u - u_{\text{nom}}) + \rho^\top \rho \quad (48)$$

$$\nabla_x h(x, t)^\top u + \frac{\partial h(x, t)}{\partial t} \geq -\alpha(h(x, t)) \quad (49)$$

$$H(x, t)^\top (I - \frac{r(x, t) \nabla_x h(x, t)^\top}{\nabla_x h(x, t)^\top r(x, t)}) (u - u_{\text{nom}}) = \rho \quad (50)$$

Reference-MCBF-QP, compared with regular CBF-QP, improves the performance of the optimization-based safe controller for star-shaped unsafe sets by reducing local minimum numbers. The new method ensures that the safe control outputs will never lead to undesirable equilibria, except when \dot{x}_{nom} is inversely collinear with the reference direction $r(x, t)$. The added constraints are designed to be of linear equality types and, thus would not cause large runtime increases. Additionally, the employment of relaxation parameter ρ sustains the feasibility of the regular CBF-QP, i.e. given the same x, t , Reference-MCBF-QP will be feasible if and only if the CBF-QP without constraints (47) and (50) is feasible. The performance of fully-actuated reference MCBF-QP in star-shaped obstacle environments is validated in **Figure 7**.

Explicit Solutions of Reference-Mod-DS: When there is only one unsafe set in the environment and robot actuation limit is ignored, like CBF-QP, explicit solutions can also be derived for Reference MCBF-QP. In the following paragraph, we derive the explicit solutions of reference MCBF-QP for fully-actuated systems in (48). The acquired result is then compared against **Theorem 5.6** to demonstrate the new method's ability

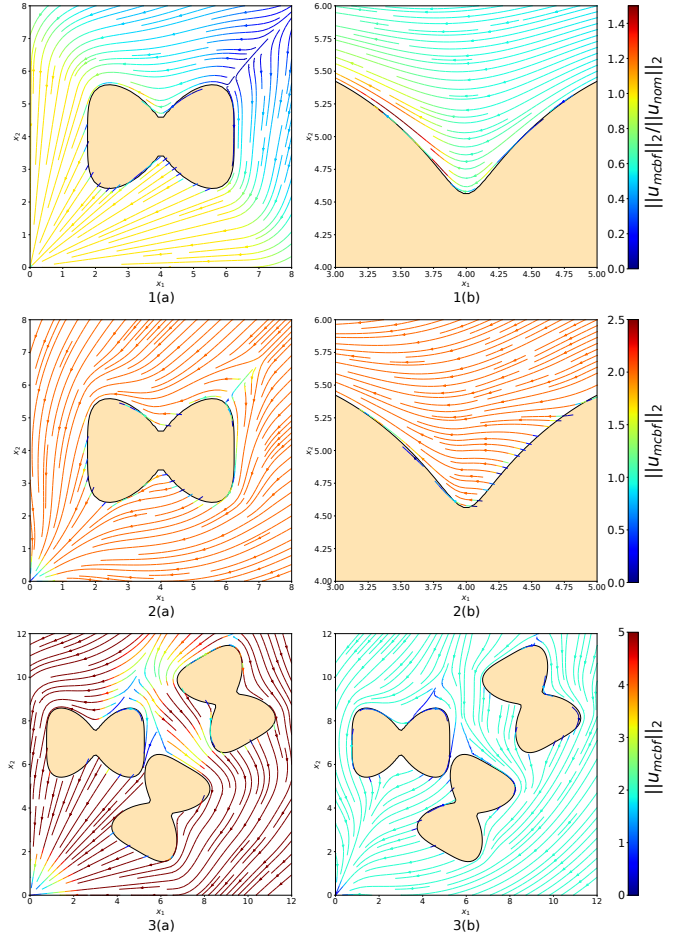


Fig. 7: Performance of reference MCBF-QP in single obstacle avoidance with no robot input constraints (first row, (a): full view, (b): close view), in single obstacle avoidance with robot input constraints of $\|u_{\text{mcbf}}\|_2 \leq 2$ (second row, (a): full view, (b): close view), and in multi-obstacle avoidance respectively with and without robot input constraints of $\|u_{\text{mcbf}}\|_2 \leq 2$ (third row (a) and (b)).

in reducing undesirable equilibria.

Derivation: Here we abuse notation and let $\alpha = \alpha(h(x, t)) - \frac{\partial h(x, t)}{\partial t}$, $H = H(x, t)$, $r = r(x, t)$, and $\nabla_x h = \nabla_x h(x, t)$. MCBF-QP in (48) can be reformulated into Lagrangian function in (51), where $\mu_{\text{eq}} \in \mathbb{R}^{d-1}$ and μ_{cbf} are the Lagrange multipliers.

$$\begin{aligned} & L(u, \rho, \mu_{\text{eq}}, \mu_{\text{cbf}}) \\ &= (u - u_{\text{nom}})^\top (u - u_{\text{nom}}) + \rho^\top \rho \\ &+ \mu_{\text{eq}}^\top [\rho - H^\top (I - \frac{r \nabla_x h^\top}{\nabla_x h^\top r}) (u - u_{\text{nom}})] - \mu_{\text{cbf}} (\nabla_x h^\top u + \alpha) \end{aligned} \quad (51)$$

According to Karush–Kuhn–Tucker theorem, the necessary and sufficient conditions for u_{mcbf} and ρ^* to be the solution to

the MCBF-QP are

$$\begin{cases} \nabla L(u_{\text{mcbf}}, \rho^*, \mu_{\text{eq}}, \mu_{\text{cbf}}) = \mathbf{0} & \text{stationarity} \\ \nabla_x h^\top u_{\text{mcbf}} + \alpha \geq 0 \\ H^\top (I - \frac{r \nabla_x h^\top}{\nabla_x h^\top r})(u_{\text{mcbf}} - u_{\text{nom}}) = \rho^* & \text{primal feasibility} \\ \mu_{\text{cbf}} \geq 0 & \text{dual feasibility} \\ \mu_{\text{cbf}}(\nabla_x h^\top u_{\text{mcbf}} + \alpha) = 0 & \text{complementary slackness} \end{cases} \quad (52)$$

Solving the linear systems in (52), the explicit expanded solution $V = [u_{\text{mcbf}}; \mu_{\text{cbf}}] \in \mathbb{R}^{d+1}$ of the MCBF-QP is computed to be

$$V = \begin{cases} \begin{bmatrix} u_{\text{nom}} \\ 0 \end{bmatrix} & \text{if } \nabla_x h^\top u_{\text{nom}} + \alpha \geq 0 \\ \begin{bmatrix} F & -\nabla_x h \\ \nabla_x h^\top & 0 \end{bmatrix}^{-1} \begin{bmatrix} F u_{\text{nom}} \\ -\alpha \end{bmatrix} & \text{otherwise} \end{cases}, \quad (53)$$

where matrix F is defined as

$$F = 2[I + (I - \frac{r \nabla_x h^\top}{\nabla_x h^\top r})^\top (I - \frac{r \nabla_x h^\top}{\nabla_x h^\top r})]. \quad (54)$$

Simplifying the above equation, the expanded explicit solution V can be written as

$$V = \begin{cases} \begin{bmatrix} u_{\text{nom}} \\ 0 \end{bmatrix} & \text{if } \nabla_x h^\top u_{\text{nom}} + \alpha \geq 0 \\ \begin{bmatrix} F^{-1}(I + \nabla_x h A) & -A^\top \\ A & -\frac{AF \nabla_x h}{\nabla_x h^\top \nabla_x h} \end{bmatrix} \begin{bmatrix} F u_{\text{nom}} \\ -\alpha \end{bmatrix} & \text{otherwise} \end{cases} \quad (55)$$

In other words, the explicit solution u_{mcbf} becomes

$$u_{\text{mcbf}} = \begin{cases} u_{\text{nom}} & \text{if } \nabla_x h^\top u_{\text{nom}} + \alpha \geq 0 \\ F^{-1}(I + \nabla_x h A) F u_{\text{nom}} + A^\top \alpha & \text{otherwise} \end{cases}, \quad (56)$$

where matrix A is defined as

$$A = -\frac{\nabla_x h^\top F^{-1}}{\nabla_x h^\top F^{-1} \nabla_x h}. \quad (57)$$

From Figure 5b, it is noticeable that vector $r(x, t)$ can be represented as a weighted vector sum of $n(x, t)$ and a vector $\sum_{i=1}^{d-1} w_i e_i$ parallel to the hyperplane $H(x, t)$ (58), $w_i \in \mathbb{R}$. Like before, we denote $e_i = e_i(x, t)$ and $n = n(x, t)$ to simplify the math. Note that $\sum_{i=0}^{d-1} (w_i)^2 = 1$ because by definition, $\|r\|_2 = 1$.

$$r = w_0 n + \sum_{i=1}^{d-1} w_i e_i \quad \text{and} \quad \sum_{i=0}^{d-1} (w_i)^2 = 1 \quad (58)$$

Based on the relationship between n and $\nabla_x h$ given in (17), $\nabla_x h = \|\nabla_x h\|_2 n$. Plug the new representation of r and $\nabla_x h$ into (54), F can be orthogonally diagonalized as the following,

where $E = E(x, t)$ is defined in (16) with $d(x, t)$ in (17).

$$\begin{aligned} F &= 4I + 2\left(\frac{1}{(w_0)^2} - 2\right)nn^\top - \frac{2}{w_0} \sum_{i=1}^{d-1} w_i (n e_i^\top + e_i n^\top) \\ &= 4EIE^\top + E \begin{bmatrix} \frac{2}{(w_0)^2} - 4 & -\frac{2w_1}{w_0} & \dots & -\frac{2w_{d-1}}{w_0} \\ -\frac{2w_1}{w_0} & 0 & \dots & 0 \\ \vdots & \vdots & \dots & \vdots \\ -\frac{2w_{d-1}}{w_0} & 0 & \dots & 0 \end{bmatrix} E^\top \\ &= E\Lambda E^\top, \end{aligned} \quad (59)$$

where

$$\Lambda = \begin{bmatrix} \frac{2}{(w_0)^2} & -\frac{2}{w_0} W^\top \\ -\frac{2}{w_0} W & 4I_{d-1} \end{bmatrix} \quad \text{and} \quad W = \begin{bmatrix} w_1 \\ \vdots \\ w_{d-1} \end{bmatrix}. \quad (60)$$

Therefore, due to the property of orthogonal diagonalization,

$$F^{-1} = (E\Lambda E^\top)^{-1} = E\Lambda^{-1}E^\top. \quad (61)$$

Given Λ is a block matrix partitioned into four blocks, it can be inverted blockwise.

$$\Lambda^{-1} = \begin{bmatrix} k & \frac{k}{2w_0} W^\top \\ \frac{k}{2w_0} W & \frac{1}{4} I_{d-1} + \frac{k}{4(w_0)^2} WW^\top \end{bmatrix}, \quad (62)$$

where given $W^\top W = \sum_{i=1}^{d-1} (w_i)^2 = 1 - (w_0)^2$,

$$k = \left(\frac{2}{(w_0)^2} - \frac{1}{(w_0)^2} W^\top W\right)^{-1} = \frac{(w_0)^2}{1 + (w_0)^2}. \quad (63)$$

Plugging in results from (61), (62) and (63) into (57),

$$A = \frac{1}{2\|\nabla_x h\|_2} (n^\top + \frac{1}{w_0} r^\top). \quad (64)$$

Therefore, when $\nabla_x h^\top u_{\text{nom}} + \alpha < 0$, the explicit solution of reference MCBF-QP u_{mcbf} can be simplified to,

$$\begin{aligned} &u_{\text{mcbf}} \\ &= \begin{cases} u_{\text{nom}} & \text{if } \nabla_x h^\top u_{\text{nom}} + \alpha \geq 0 \\ u_{\text{nom}} - \frac{1}{2w_0} (w_0 nn^\top + r n^\top) u_{\text{nom}} + A^\top \alpha & \text{otherwise} \end{cases}. \end{aligned} \quad (65)$$

Remark: The explicit solution of regular CBF-QP in fully-actuated systems (13) can be rewritten using n as the following. Note that $nn^\top u_{\text{nom}} = n^\top u_{\text{nom}} n$ for all $n, u_{\text{nom}} \in \mathbb{R}^d$.

$$u_{\text{cbf}} = \begin{cases} u_{\text{nom}} & \text{if } \nabla_x h^\top u_{\text{nom}} + \alpha \geq 0 \\ u_{\text{nom}} - (nn^\top u_{\text{nom}} + \alpha \frac{n}{\|\nabla_x h\|_2}) & \text{otherwise} \end{cases} \quad (66)$$

Given the explicit solution of the proposed reference MCBF-QP in (65), the differences between the outputs of the two solutions can be quantified as in (67).

$$\begin{aligned} &u_{\text{mcbf}} - u_{\text{cbf}} \\ &= \begin{cases} 0 & \text{if } \nabla_x h^\top u_{\text{nom}} + \alpha \geq 0 \\ -\frac{1}{2w_0} (r - w_0 n) n^\top u_{\text{nom}} + (A^\top + \frac{n}{\|\nabla_x h\|_2}) \alpha & \text{otherwise} \end{cases} \end{aligned} \quad (67)$$

When the controlled agent is on the boundary of the unsafe

sets, i.e. $\alpha = 0$, (67) becomes

$$u_{\text{mcbf}} - u_{\text{cbf}} = \begin{cases} 0 & \text{if } \nabla_x h^\top u_{\text{nom}} \geq 0 \\ -\frac{1}{2w_0}(r - w_0n)n^\top u_{\text{nom}} & \text{otherwise} \end{cases} \quad (68)$$

Given (58), we know $n^\top r = w_0$ and $e_i^\top r = w_i$ for $i \in \{1, 2, \dots, d-1\}$. Therefore, the quantitative relationship between reference Mod-DS and regular CBF-QP deduced in (39) can be reformulated as

$$u_{\text{mod}}^r - u_{\text{cbf}} = \begin{cases} 0 & \text{if } \nabla_x h^\top u_{\text{nom}} \geq 0 \\ -\frac{\lambda_e - \lambda}{w_0}(r - w_0n)n^\top u_{\text{nom}} & \text{otherwise} \end{cases} \quad (69)$$

Since λ, λ_e can be any real number satisfying (18), there exist an infinite amount of λ, λ_e meeting the requirement $\lambda_e - \lambda = \frac{1}{2}$. Therefore, the conclusion can be drawn that there always exist feasible λ, λ_e pairs such that outputs from reference MCBF-QP equal that from reference Mod-DS on boundaries of the unsafe sets. This guarantees that reference MCBF-QP is free of undesirable equilibria except when u_{nom} is inversely collinear to $r(x, t)$ in the boundary set ∂C .

B. On-Manifold MCBF for Non-star-shaped Obstacle Mod-Avoidance

By keeping CBF constraints in regular CBF-QP to account for Mod-DS's policies in $n(x, t)$ direction and introducing new constraints (47) and (50) to mimic reference Mod-DS's actions in the tangent hyperplane $H(x, t)$, reference MCBF-QP successfully combines the strength of both and realizes star-shaped obstacle avoidance using QP-based methods. While on-manifold Modulation, functioning under the aggregate effects of 3 policies, is too structurally complicated to be explicitly connected to CBF-QP on the theory level, its main component, like other Mod-DS approaches, modulates \dot{x} in $n(x, t)$ direction similar to CBF constraints and prevents the formation of undesirable equilibrium by ordering the directions of \dot{x} projected onto the tangent hyperplane $H(x, t)$ using $\phi(x, t)$. Therefore, by introducing $H(x, t)$ related constraints, inspired by $\phi(x, t)$ in on-manifold Mod-DS, into CBF-QP, on-manifold MCBF-QP is constructed to achieve local-minimum-free safe control for control affine systems in general (VII-B). The parameter γ is a user-defined positive real number, i.e. $\gamma \in \mathbb{R}^+$. Unlike reference MCBF-QP, which stays feasible as long as the CBF-QP without constraint (47) is feasible, on-manifold MCBF-QP's feasible domain is always smaller than that of the CBF-QP without constraint (71). Additionally, the larger γ is, the smaller the feasible domain of on-manifold MCBF-QP will be. The performance of on-manifold MCBF-QP in concave obstacle environments is validated in Figure 8.

$$u_{\text{mcbf}} = \arg \min_{u \in \mathbb{R}^p} (u - u_{\text{nom}})^\top (u - u_{\text{nom}})$$

$$L_f h(x, t) + L_g h(x, t)u + \frac{\partial h(x, t)}{\partial t} \geq -\alpha(h(x, t)) \quad (70)$$

$$\phi(x, t)^\top f(x) + \phi(x, t)^\top g(x)u \geq \gamma \quad (71)$$

For fully-actuated systems in (10), the special case of CBF-

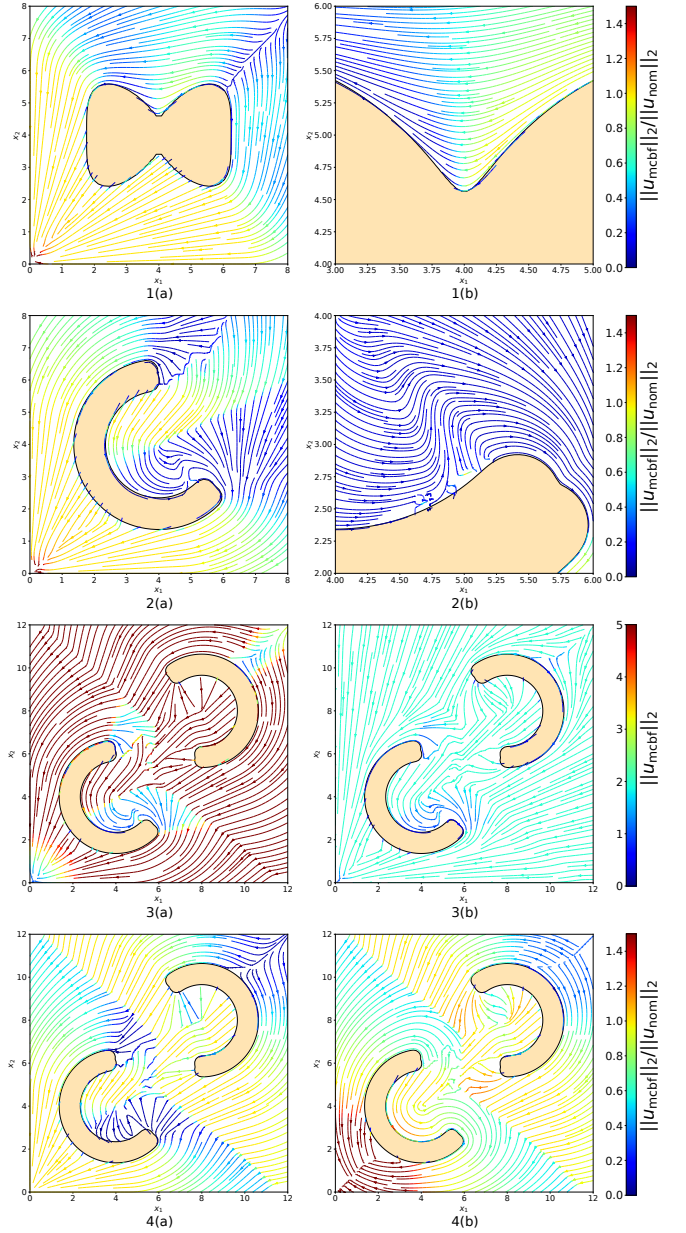


Fig. 8: Performance of on-manifold MCBF-QP in single star-shaped (first row) and non-star-shaped (second row, (a): full view, (b): close view) obstacle avoidance with no robot input constraints, in multi-concave obstacle avoidance (third row, (a): without input constraints, (b): with robot input constraints of $\|u_{\text{mcbf}}\|_2 \leq 2$), given $\gamma = 1$. Lastly, pictures on the fourth row show the effects of γ sizes on the resulted safe trajectories ((a): $\gamma = 0.1$, (b): $\gamma = 10$).

QP can be simplified as in (VII-B).

$$u_{\text{mcbf}} = \arg \min_{u \in \mathbb{R}^d, \rho \in \mathbb{R}^{d-1}} (u - u_{\text{nom}})^\top (u - u_{\text{nom}})$$

$$\nabla_x h(x, t)^\top u + \frac{\partial h(x, t)}{\partial t} \geq -\alpha(h(x, t)) \quad (72)$$

$$\phi(x, t)^\top u \geq \gamma \quad (73)$$

Remark: While reference MCBF-QP can be in theory extended to nonlinear dynamical systems with equations in

(VII-A), its applications in high dimensional systems is limited because finding reference directions $r(x, t)$ when $d > 3$ is nontrivial in general and its complexity scales up as d increases. However, given proper step size β , the geodesic approximation method in (22) is able to closely approximate unsafe set boundaries for any given state $x \in \mathbb{R}^d$. As a result, on-manifold MCBF-QP can be readily applied in any control affine robot system.

VIII. ROBOT EXPERIMENT

In this section, the obstacle avoidance performances using MCBF-QPs proposed in section VII are validated in fully actuated and underactuated control affine systems, using respectively omnidirectional-drive Ridgeback and differential-drive Fetch robots. The constraint-enforcing effects of the modified Mod-DS methods proposed in section VI are also examined using Ridgeback robot in gazebo simulations.

A. Simulation Environment Setup

In this work, a realistic hospital environment, featuring convex and concave static furniture as well as nurses and patients walking around as obstacles, is set up to validate the Mod-based CBF-QP variants proposed and compare them against existing approaches of Mod-DS and CBF-QP. Based on differences in robot initial and target locations, 5 scenarios are designed as in Figure 9a. In each scenario, the robot is provided with the task of traveling from the initial position to the target while avoiding collisions with obstacles in the path. The designed scenarios well represent the encounterment a delivery robot needs to face when working in crowded dynamic environments like the hospital. Scenario 1 tests the controller's ability to navigate reactively out of a complicated concave obstacle like the front desk; scenario 2 and 3 (denote as mix and mix-reverse in Table III) challenged the robots with a mix of concave and convex obstacles; lastly, scenario 4 and 5 test robot's performances facing convex obstacles, the benches. Robots are assumed to process full knowledge of obstacles within a 3-meter detecting range inside the lobby during planning, including part of the static map shown in Figure 9 and the real-time poses of the humans, modeled as cylinders, from a motion capture system.

B. Robot Dynamics

In tests using fully actuated systems, the performances of the proposed reference and on-manifold MCBF-QP methods in 2-dimensional Euclidean space (R-MCBF-QP and onM-MCBF-QP) compete against regular CBF-QP and the proposed constrained Mod-DS using standard Ridgeback dynamics below.

$$\begin{bmatrix} \dot{x} \\ \dot{y} \end{bmatrix} = \begin{bmatrix} u_x \\ u_y \end{bmatrix} \quad (74)$$

In tests for underactuated control affine systems, the performance of the proposed on-manifold MCBF-QP method in 2-dimensional Euclidean space (shifted on-manifold Mod-based CBF-QP, S-onM-MCBF) competes against regular CBF-QP

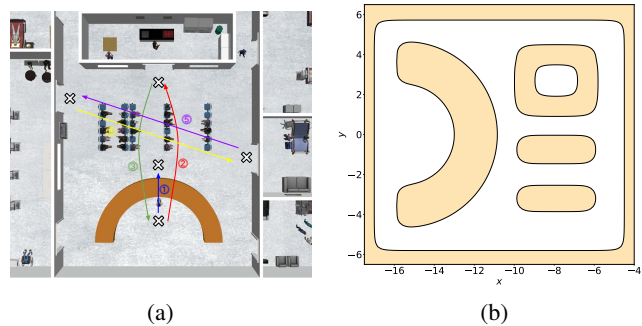


Fig. 9: Simulation environment and controller setup for robot comparison tests. Figure 9a displays the 5 scenarios designed for robot tests and Figure 9b illustrates the robot's knowledge of the hospital environment.

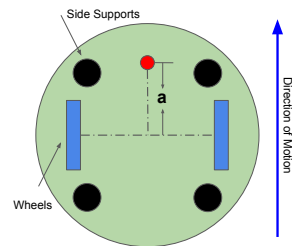


Fig. 10: Modified point of interest on Fetch robot.

using the shifted unicycle model (shifted CBF-QP, S-CBF-QP), while on-manifold MCBF-QP method's performance in 3-dimensional non-Euclidean space (high order on-manifold Mod-based CBF-QP, HO-onM-MCBF) competes against higher order CBF-QP (HO-CBF-QP) using Fetch dynamics. The most commonly used model for differential drive robots like Fetch is the unicycle model below.

$$\dot{\xi} = \begin{bmatrix} \dot{x} \\ \dot{y} \\ \dot{\theta} \end{bmatrix} = \begin{bmatrix} \cos \theta & 0 \\ \sin \theta & 0 \\ 0 & 1 \end{bmatrix} \begin{bmatrix} v \\ \omega \end{bmatrix} \quad (75)$$

While CBF-QP is easily generalizable to any control affine systems, it suffers from one critical restriction: the CBF has to be of relative degree 1. In other words, the CBF's first time-derivative has to depend on the control input. Since the control input ω in the standard unicycle model is of relative degree 2 to the CBFs h_{conv} , h_{star} and h_{nstar} in subsection II-C, we chose a point of interest $a > 0$ m ahead of the wheel axis of Fetch, instead of robot center, as shown in Figure 10. The unicycle dynamics with the shifted coordinate system becomes the following.

$$\dot{\xi} = \begin{bmatrix} \dot{x} \\ \dot{y} \\ \dot{\theta} \end{bmatrix} = \begin{bmatrix} \cos \theta & -a \sin \theta \\ \sin \theta & a \cos \theta \\ 0 & 1 \end{bmatrix} \begin{bmatrix} v \\ \omega \end{bmatrix} \quad (76)$$

Because h_{conv} , h_{star} and h_{nstar} 's partial derivative with respect to θ are all zeros. The CBF constraints for the shifted unicycle system, adopted by shifted CBF-QP (S-CBF-QP) and 2-dimensional shifted on-manifold MCBF-QP (S-onM-MCBF-

QP) methods, can be written as

$$\frac{\partial h(x, y, t)}{\partial x} \dot{x} + \frac{\partial h(x, y, t)}{\partial y} \dot{y} + \frac{\partial h(x, y, t)}{\partial t} \geq -\alpha(h(x, y, t)). \quad (77)$$

While the shifted unicycle model enables CBFs to be defined as signed distance functions like h_{conv} , h_{star} and h_{nstar} , the method cannot be easily generalized to all underactuated robots. HO-CBF-QP solves the generalizability issue by using high order control barrier functions (HO-CBFs) $h_{\text{OH}}(\xi, t)$ of relative degree 1 to control inputs, instead of signed distance functions $h(x, y, t)$ as CBFs. Here, we demonstrate that the on-manifold MCBF-QP method we proposed, likewise can be generalized to high-relative-order robot dynamics by controlling Fetch through the standard unicycle model in (75) using high-order on Manifold Mod-based CBF-QP (HO-onM-MCBF). HO-CBF $h_{\text{OH}}(\xi, t)$ used by 3-dimensional HO-onM-MCBF and HO-CBF-QP in our validations are constructed as the following, where $w \in \mathbb{R}^+$.

$$h_{\text{OH}}(\xi, t) = h(x, y, t) + w \frac{\partial h(x, y, t)}{\partial x} \cos \theta + w \frac{\partial h(x, y, t)}{\partial y} \sin \theta \quad (78)$$

Nominal Controller: For fully-actuated systems, nominal controllers u_{nom}^l in (23) with $\epsilon = \frac{1}{\|x\|_2}$ are used by Ridgeback. For underactuated systems, the nominal controllers are approximated from the linear dynamical systems as the following, where ψ is the angle difference between the current robot pose θ and the desired robot pose estimated using the orientation of u_{nom}^l , and Δt is the update timestep of the nominal controller. The approximation is not exact due to the non-holonomic property of differential drive systems.

$$u_{\text{nom}} = \|u_{\text{nom}}^l\|_2 \quad \omega_{\text{nom}} = \frac{\psi}{\Delta t} \quad (79)$$

C. Geodesic Approximation in Non-Euclidean Space

[16] shows that the obstacle exit strategy of geodesic approximation, given well-tuned step size β and horizon size N , can generate a first-order approximation to the obstacle surface in Euclidean space \mathbb{R}^d alongside an effective circumventing strategy, connecting robot current position to target position with the least reward P_N . In this work, we demonstrate that such a strategy can be extended to non-Euclidean space, by replacing x_i with ξ_i , when used in Mod-based CBF-QP, making possible local-minimum-free control affine CBF-QP in general.

Here, the application of the geodesic approximation strategy is validated using the 3-dimensional non-Euclidean state space for the unicycle model $[x, y, \theta]$. Figure 11(a), (b) and (c) shows what the unsafe region defined by HO-CBF in Equation 78 looks like in our constructed 3D non-Euclidean space. For visual effects and interpretability of the obstacle, only the section with $\theta \in [0, 2\pi)$ is shown. Given robot initial state $\xi_0 = [3, 3, 0]$ and 20 e^0 vectors evenly distributed in the plane tangent to the gradient of obstacle $h_{\text{OH}}(\xi_0, t)$, geodesic approximation strategy, as shown in Figure 11, is able to select the circumventing trajectories traveling most efficiently towards the target using reward function $p(\xi_i, x^*) = \|\xi_i[:2] - x^*\|_2$.

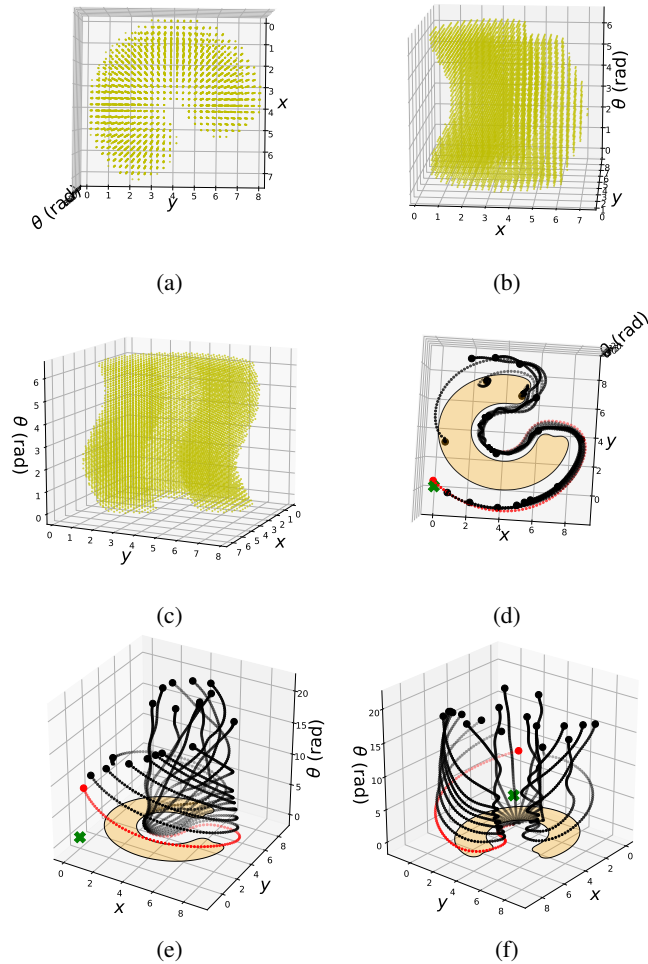


Fig. 11: Figure 11a, Figure 11b, and Figure 11c shows the top, side and diagonal views of the unsafe spaces defined by the constructed high order barrier function h_{OH} (78). Figure 11d, Figure 11e, and Figure 11f demonstrate from 3 view angles that the geodesic approximation method can be adapted to find the most effective circumventing strategy (colored in red) to the target location (denoted by green 'X'), despite the state space being non-euclidean.

D. Simulation Results

The performances of the proposed Mod-based CBF-QP methods are validated in simulation environments through comparisons to existing reactive safe controllers, including comparing R-MCBF-QP and onM-MCBF-QP with normal Mod-DS (N-Mod-DS), reference Mod-DS (R-Mod-DS), on-manifold Mod-DS (onM-Mod-DS) and CBF-QP for fully-actuated systems in gazebo hospital environments using Ridgeback, competing S-onM-MCBF-QP against S-CBF-QP for underactuated differential drive systems using Fetch in gazebo hospital environments, and lastly matching HO-onM-MCBF-QP with HO-CBF-QP in the underactuated control affine system of standard unicycle model from (75) in python-simulated hospital environments. The speed-constraining strategy for Mod-DS approaches proposed in section VI is validated on N-Mod-DS, R-Mod-DS, and onM-Mod-DS for fully actuated

			Static				Dynamic		
	Method	Environment	Duration (s)	Safe %	Reached %	Infeasible #	Safe %	Reached %	Infeasible #
Fully Actuated Systems	N-Mod-DS	concave	NA	1.00	0.00	202	1.00	0.00	223
		convex	19.9s	1.00	1.00	2	0.50	1.00	90
		mix	NA	1.00	0.00	207	1.00	0.00	219
		mix-reverse	NA	1.00	0.00	7	0.00	0.00	106
	R-Mod-DS	concave	NA	1.00	0.00	19	1.00	0.00	20
		convex	17.4 s	1.00	1.00	5	1.00	1.00	9
		mix	NA	1.00	0.00	20	1.00	0.00	20
		mix-reverse	21.7 s	1.00	1.00	9	1.00	1.00	14
	OnM-Mod-DS	concave	16.2 s	1.00	1.00	7	1.00	1.00	30
		convex	15.7 s	1.00	1.00	2	1.00	1.00	85
		mix	21.3 s	1.00	1.00	6	1.00	1.00	10
		mix-reverse	21.7 s	1.00	1.00	9	1.00	1.00	23
	CBF-QP	concave	NA	1.00	0.00	0	1.00	0.00	0
		convex	33.7 s	1.00	1.00	0	1.00	1.00	1
		mix	NA	1.00	0.00	0	1.00	0.00	0
		mix-reverse	NA	1.00	0.00	0	1.00	0.00	0
	R-MCBF-QP	concave	NA	1.00	0.00	0	1.00	0.00	0
		convex	29.5 s	1.00	1.00	0	1.00	1.00	0
mix		NA	1.00	0.00	0	1.00	0.00	0	
mix-reverse		38.2S	1.00	1.00	0	1.00	1.00	0	
onM-MCBF-QP	concave	22.8 s	1.00	1.00	0	1.00	1.00	0	
	convex	25.8 s	1.00	1.00	0	1.00	1.00	0	
	mix	27.2 s	1.00	1.00	0	1.00	1.00	0	
	mix-reverse	33.3 s	1.00	1.00	0	1.00	1.00	0	
Underactuated Systems	S-CBF-QP	concave	NA	1.00	0.00	0	1.00	0.40	0
		convex	17.8 s	1.00	1.00	0	0.95	1.00	1
		mix	24.3 s	1.00	1.00	0	0.70	0.70	24
		mix-reverse	19.9 s	1.00	1.00	0	1.00	1.00	0
	S-onM-MCBF-QP	concave	16.8 s	1.00	1.00	0	0.80	0.80	0
		convex	16.1 s	1.00	1.00	0	1.00	1.00	0
		mix	21.3 s	1.00	1.00	0	1.00	1.00	0
		mix-reverse	20.4 s	1.00	1.00	0	1.00	1.00	0
	HO-CBF-QP	concave	NA	1.00	0.00	0	1.00	0.00	0
		convex	16.1s	1.00	1.00	0	1.00	1.00	10
		mix	21.5s	1.00	1.00	0	0.60	0.90	248
		mix-reverse	21.4s	1.00	1.00	0	1.00	1.00	0
	HO-onM-MCBF-QP	concave	15.8s	1.00	1.00	0	1.00	1.00	0
		convex	18.1s	1.00	1.00	0	1.00	1.00	3
		mix	22.8s	1.00	1.00	0	1.00	1.00	0
		mix-reverse	23.0s	1.00	1.00	0	1.00	1.00	0

TABLE III: Performance of Mod-DS, CBF-QP and Mod-based CBF-QP approaches, running at 20 Hz, measured by the duration of the produced trajectories, safety rate (collision-free rate), the rate for the robot to reach the target locations successfully, and the average number of infeasibility encountered, in simulated hospital environments.

systems. Controllers in all simulations are running at 20Hz and those in all real-life experiments are running at 50Hz. In gazebo-simulated environments, the robot is asked to repeat the task of traveling from a fixed initial pose to the target 10 times. In python-simulated environments, the robot’s performances starting from the same initial location but with 10 different orientations are recorded. The recorded performances are analyzed using the time (in seconds) that the robot takes to travel from the initial to the target locations (durations), the percentage of collision-free trajectories among the repeated ones (safe %), the chance for the robot to reach the target (reached %), and the average number of unsolvable cases (infeasibility) encountered by the controller per trajectories in [Table III](#). Note the metric duration cannot be computed for trajectories where the robot is stuck in local minima and fails to reach the target, and are instead denoted as not applicable (“NA”).

Based on the data collected, the following conclusion can be drawn: in fully actuated systems, Mod-DS approaches like N-Mod-DS, R-Mod-DS, and onM-Mod-DS run faster than CBF-QP-based approaches like CBF-QP, R-MCBF-QP and onM-MCBF-QP, which matches the observation made in [Table II](#) that Mod-DS approaches have faster near-obstacle velocities. While both methods guarantee robot safety by decelerating

in the direction normal to the obstacles, common Mod-DS approaches additionally accelerate in the tangent direction, leading to a shorter duration. However, the weakness of Mod-DS approaches is that achieving multi-obstacle avoidance using the weighted sum of the stretched velocities computed with respect to each obstacle cannot handle well the scenarios where the robot is squeezed between multiple extremely close obstacles. Therefore, N-Mod-DS, R-Mod-DS and onM-Mod-DS have significantly higher chances of infeasibility in crowded environments like the simulated hospital in comparison to the other CBF-based methods. The encounterment of controller infeasibility drives N-Mod-DS to collision in some dynamic simulations, while CBF-QP, proven to be theoretically equivalent to N-Mod-DS in single obstacle avoidance in [Theorem 5.4](#), does not suffer from such issues. However, in terms of the ability to reach the target, the performances of Mod-DS approaches like R-Mod-DS and onM-Mod-DS are superior to that of the CBF-QP. CBF-QP is recorded to stop at local minimum in all non-convex environments, while R-Mod-DS is able to successfully navigate through mix-reverse environment and onM-Mod-DS is completely local-minimum free. The performances of the Mod-based CBF-QPs we proposed, R-MCBF-QP and onM-MCBF-QP, are demonstrated to be superior to both Mod-DS and CBF-QP.

They well combine the robust safety guarantee of CBF-QP with local minimum elimination of R-Mod-DS and onM-Mod-DS to achieve little solver infeasibility, high safety and convergence guarantees with comparable runtime.

In underactuated differential drive systems, both regular CBF-QP methods, such as S-CBF-QP and HO-CBF-QP, and proposed Mod-based approaches like S-onM-MCBF-QP and HO-onM-MCBF-QP provide decent safety guarantees and will only collide with obstacles when solver infeasibility happens. Yet both proposed Mod-DS approaches are demonstrated to significantly increase the chances of reaching the goal in concave environments. Furthermore, in most case scenarios, Mod-based CBF-QP approaches have shorter durations because the tangent velocity control incorporated from onM-Mod-DS ensures leading the robot towards the more efficient paths.

In conclusion, tests in simulated hospital environments show that the performances of the proposed Mod-based CBF-QP approaches exceed those of Mod-DS and CBF-QP methods in both fully actuated and underactuated control affine systems.

E. Real World Experiments

In addition to simulations, the proposed S-onM-MCBF-QP and HO-onM-MCBF-QP methods are compared to S-CBF-QP and HO-CBF-QP in real-life experiments using Fetch given nominal controller in (79). In the first experiment, Fetch is challenged to reach the goal position on the other side of the room despite active attempts from a walking human to block its path. In the second experiment, the robot is tasked to navigate out of a C-shaped cluster region towards the target. All experiments are repeated 5 times with different robot initial poses in static scenarios and different human walking trajectories in dynamic scenarios. The results demonstrate that CBF-induced local minima will deteriorate robot task completion performance, while the introduction of onM-Mod-based constraints into the same QP problem can sufficiently eliminate those local minima. In 2D navigation tasks using Fetch, though both HO-onM-MCBF-QP and S-onM-MCBF-QP drastically improve robot task completion performance, S-onM-MCBF-QP using the shifted unicycle model outperforms HO-onM-MCBF-QP using the standard unicycle model in terms of path efficiency and task completion rate. The reason for that is the unsafe region defined by HOCBF h_{OH} (78), as shown in Figure 11c, is not the same as the actual obstacle region, causing the geodesic approximation strategy to output sometimes non-optimal choices of tangent vectors $\phi(\xi, t)$ for the robot to track. Additionally, finding appropriate step size β and horizon N to use during geodesic approximation are more challenging for HO-MCBF-QP that searches for $\phi(\xi, t)$ in 3D non-Euclidean state spaces, compared with S-MCBF-QP that looks for $\phi(x, y, t)$ instead in the 2D Euclidean state spaces. However, HO-onM-MCBF-QP's merit is its generalizability which can be theoretically adopted by all robot models.

IX. DISCUSSION AND FUTURE DIRECTIONS

By quantitatively and analytically comparing the performances of optimization-based safe control approaches of CBF-QP, the closed-form solutions from Mod-DS and the Mod-based CBF-QP methods we propose in both static and moving

Scenario	Methods	Safe %	Reached %	Duration (s)
convex dynamic	S-CBF	100	0	NA
	S-onM-MCBF	100	100	12.4
	HO-CBF	100	0	NA
	HO-onM-MCBF	100	100	14.3
static concave	S-CBF	100	0	NA
	S-onM-MCBF	100	100	14.9
	HO-CBF	100	0	NA
	HO-onM-MCBF	100	80	30.7

TABLE IV: Performances of proposed onManifold-Mod-based CBF-QP methods in comparison to CBF-QP formulations in real-life experiments using Fetch at 20Hz.

obstacle environments, the following conclusion can be drawn for obstacle avoidance in 2-dimensional space using single-integrator and differential drive systems:

- 1) Mod-DS approaches like reference Mod-DS and on-manifold Mod-DS perform better with concave obstacles by causing fewer undesirable equilibria on the boundary set ∂C than CBF-QP in static and less crowded dynamic environments.
- 2) CBF-QP handles safety guarantees better than Mod-DS in crowded dynamic environments. However, its convergence to targets cannot be guaranteed in environments with concave obstacles.
- 3) In comparison to Mod-DS and CBF-QP, Mod-based CBF-QP performs better in vast majority of the cases, no matter the systems are fully-actuated or underactuated. However, even with the use of jax, current update frequency of the controller is limited to 50Hz and will decrease as the robot dynamics gets more complicated with larger state vector ξ . In applications where a higher update frequency using fully-actuated systems is desired, using on-manifold Mod-DS in combination of constrained Mod-DS strategies will be a good alternative.

In this work, the proposed Mod-based CBF-QP methods are validated using omni-directional and differential drive robot dynamics. However, in addition to locomotion tasks, robot arm manipulation's performance is also degraded by the existence of local minima in concave joint spaces. Therefore, adapting the on-manifold Mod-based CBF-QP methods to achieve local-minimum-free manipulation would be one future directions for us to explore. Besides, the performance of the tangent direction selection using geodesic approximation strategy relies on proper user tuning of β , and N parameters. Automating the tuning process using analytic or machine-learning based algorithms to enable Mod-based CBF-QPs to navigate local-minimum-free around constantly deforming dynamic obstacles would be another future direction for the project.

REFERENCES

- [1] P. A. Lasota, T. Fong, and J. A. Shah, "A survey of methods for safe human-robot interaction," *Foundations and Trends® in Robotics*, vol. 5, no. 4, pp. 261–349, 2017.
- [2] A. D. Ames, S. Coogan, M. Egerstedt, G. Notomista, K. Sreenath, and P. Tabuada, "Control barrier functions:

- Theory and applications,” in *2019 18th European control conference (ECC)*. IEEE, 2019, pp. 3420–3431.
- [3] J. Zeng, B. Zhang, and K. Sreenath, “Safety-critical model predictive control with discrete-time control barrier function,” in *2021 American Control Conference (ACC)*. IEEE, 2021, pp. 3882–3889.
- [4] Y. Emam, P. Glotfelter, S. Wilson, G. Notomista, and M. Egerstedt, “Data-driven robust barrier functions for safe, long-term operation,” *IEEE Transactions on Robotics*, vol. 38, no. 3, pp. 1671–1685, 2022.
- [5] A. Singletary, S. Kolathaya, and A. D. Ames, “Safety-critical kinematic control of robotic systems,” *IEEE Control Systems Letters*, vol. 6, pp. 139–144, 2022.
- [6] M. Saveriano and D. Lee, “Learning barrier functions for constrained motion planning with dynamical systems,” in *2019 IEEE/RSJ International Conference on Intelligent Robots and Systems (IROS)*, 2019, pp. 112–119.
- [7] I. Jang and H. J. Kim, “Safe control for navigation in cluttered space using multiple lyapunov-based control barrier functions,” *IEEE Robotics and Automation Letters*, vol. 9, no. 3, pp. 2056–2063, 2024.
- [8] J. Borenstein and Y. Koren, “Real-time obstacle avoidance for fast mobile robots,” *IEEE Transactions on systems, Man, and Cybernetics*, vol. 19, no. 5, pp. 1179–1187, 1989.
- [9] E. Rimon and D. Koditschek, “Exact robot navigation using artificial potential functions,” *IEEE Transactions on Robotics and Automation*, vol. 8, no. 5, pp. 501–518, 1992.
- [10] H. J. S. Feder and J.-J. Slotine, “Real-time path planning using harmonic potentials in dynamic environments,” in *Proceedings of International Conference on Robotics and Automation*, vol. 1. IEEE, 1997, pp. 874–881.
- [11] S. M. Khansari-Zadeh and A. Billard, “A dynamical system approach to realtime obstacle avoidance,” *Autonomous Robots*, vol. 32, pp. 433–454, 2012.
- [12] M. Saveriano and D. Lee, “Distance based dynamical system modulation for reactive avoidance of moving obstacles,” in *2014 IEEE International Conference on Robotics and Automation (ICRA)*, 2014, pp. 5618–5623.
- [13] L. Huber, A. Billard, and J.-J. Slotine, “Avoidance of convex and concave obstacles with convergence ensured through contraction,” *IEEE Robotics and Automation Letters*, vol. 4, no. 2, pp. 1462–1469, 2019.
- [14] A. Billard, S. Mirrazavi, and N. Figueroa, *Learning for Adaptive and Reactive Robot Control: A Dynamical Systems Approach*. MIT Press, 2022.
- [15] A. Dahlin and Y. Karayiannidis, “Creating star worlds: Reshaping the robot workspace for online motion planning,” *IEEE Transactions on Robotics*, vol. 39, no. 5, pp. 3655–3670, 2023.
- [16] C. K. Fourie, N. Figueroa, and J. A. Shah, “On-manifold strategies for reactive dynamical system modulation with nonconvex obstacles,” *IEEE Transactions on Robotics*, vol. 40, pp. 2390–2409, 2024.
- [17] A. Singletary, K. Klingebiel, J. Bourne, A. Browning, P. Tokumaru, and A. Ames, “Comparative analysis of control barrier functions and artificial potential fields for obstacle avoidance,” in *2021 IEEE/RSJ International Conference on Intelligent Robots and Systems (IROS)*. IEEE, 2021, pp. 8129–8136.
- [18] Z. Li, “Comparison between safety methods control barrier function vs. reachability analysis,” *arXiv preprint arXiv:2106.13176*, 2021.
- [19] Y. Lin, J. McPhee, and N. L. Azad, “Comparison of deep reinforcement learning and model predictive control for adaptive cruise control,” *IEEE Transactions on Intelligent Vehicles*, vol. 6, no. 2, pp. 221–231, 2021.
- [20] S. Sakaguchi, “Star shaped coincidence sets in the obstacle problem,” *Annali della Scuola Normale Superiore di Pisa - Classe di Scienze*, vol. 11, no. 1, pp. 123–128, 1984.
- [21] D. E. Koditschek and E. Rimon, “Robot navigation functions on manifolds with boundary,” *Advances in Applied Mathematics*, vol. 11, no. 4, pp. 412–442, 1990. [Online]. Available: <https://www.sciencedirect.com/science/article/pii/019688589090017S>
- [22] G. Notomista and M. Saveriano, “Safety of dynamical systems with multiple non-convex unsafe sets using control barrier functions,” *IEEE Control Systems Letters*, vol. 6, pp. 1136–1141, 2021.
- [23] Y. Zhou, S. Booth, N. Figueroa, and J. Shah, “Rocus: Robot controller understanding via sampling,” in *Conference on Robot Learning*. PMLR, 2022, pp. 850–860.
- [24] M. F. Reis, A. P. Aguiar, and P. Tabuada, “Control barrier function-based quadratic programs introduce undesirable asymptotically stable equilibria,” *IEEE Control Systems Letters*, vol. 5, no. 2, pp. 731–736, 2021.
- [25] L. Huber, J.-J. Slotine, and A. Billard, “Avoiding dense and dynamic obstacles in enclosed spaces: Application to moving in crowds,” *IEEE Transactions on Robotics*, vol. 38, no. 5, pp. 3113–3132, 2022.

APPENDIX

A. Metrics for Collision Avoidance Evaluation

TABLE V: Metrics for Collision Avoidance Comparison [23]

Behavior Metric	Equation
Trajectory Length	$l = \int_{\mathcal{T}} 1 ds$
Average Jerk	$\bar{j} = \frac{1}{l} \int_{\mathcal{T}} \ \ddot{x}\ _2 ds$
Straight-Line Deviation	$\eta = \frac{1}{l} \int_{\mathcal{T}} \ x - \text{proj}_{x^* - x_0} x\ _2 ds$
Obstacle Clearance	$d_{\text{obs}} = \frac{1}{l} \int_{\mathcal{T}} \min_{x_o \in \neg C} \ x - x_o\ _2 ds$
Near Obstacle Velocity	$v_{\text{near}} = \frac{\int_{\mathcal{T}} \ \dot{x}\ _2 / \min_{x_o \in \neg C} \ x - x_o\ _2 ds}{\int_{\mathcal{T}} 1 / \min_{x_o \in \neg C} \ x - x_o\ _2 ds}$

B. Impenetrability of Speed and Velocity Constraining Mod-DS

Proof: In [11], [13], and [16], the unconstrained outputs u_{unc} from respectively normal, reference and on-manifold Mod-DS approaches are proven to achieve obstacle impenetrability in terms of the von Neuman boundary condition, listed in Eq. (80).

$$n(x, t)^\top u_{\text{unc}} = 0 \quad \forall x \in \partial C \quad (80)$$

Given safe controller u_{unc} in Eq. (80), we want to show that the constrained solutions u_c of the QPs in (43) and (45) also

satisfies the set invariance condition of impenetrability. In other words,

$$n(x, t)^\top u_c \geq 0 \quad \forall x \in \partial C \quad (81)$$

Since any solutions u_c from QPs in (43) and (45) must satisfy the safety constraints in (42), $n(x, t)^\top u_c \geq n(x, t)^\top u_{\text{unc}}$ must be true for all state x . This implies that $n(x, t)^\top u_c \geq 0$ if $n(x, t)^\top u_{\text{unc}} = 0$. Therefore, the statement in (81) always holds. ■